DYNAMIC STABILITY TESTING OF SPACE SHUTTLE CONFIGURATIONS DURING ABORT SEPARATION AT MACH NUMBERS 1.76 AND 2

Bob Uselton and Arthur R. Wallace

ARO, Inc.

October 1971

VON KÁRMÁN GAS DYNAMICS FACILITY

ARNOLD ENGINEERING DEVELOPMENT CENTER

AIR FORCE SYSTEMS COMMAND

ARNOLD AIR FORCE STATION, TENNESSEE

NOTICES

When U. S. Government drawings specifications, or other data are used for any purpose other than a definitely related Government procurement operation, the Government thereby incurs no responsibility nor any obligation whatsoever, and the fact that the Government may have formulated, furnished, or in any way supplied the said drawings, specifications, or other data, is not to be regarded by implication or otherwise, or in any manner licensing the holder or any other person or corporation, or conveying any rights or permission to manufacture, use, or sell any patented invention that may in any way be related thereto.

Qualified users may obtain copies of this report from the Defense Documentation Center.

References to named commercial products in this report are not to be considered in any sense as an endorsement of the product by the United States Air Force or the Government.

DYNAMIC STABILITY TESTING OF SPACE SHUTTLE CONFIGURATIONS DURING ABORT SEPARATION AT MACH NUMBERS 1.76 AND 2

Bob Uselton and Arthur R. Wallace
ARO, Inc.

FOREWORD

The work reported herein was sponsored by the Arnold Engineering Development Center (AEDC), Air Force Systems Command (AFSC), under Program Element 65802F.

The results of this work presented were obtained by ARO, Inc. (a subsidiary of Sverdrup & Parcel and Associates, Inc.), contract operator of AEDC, AFSC, Arnold Air Force Station, Tennessee, under Contract F40600-72-C-0003. The tests were conducted under ARO Project No. VT2128 on March 22 and 23, 1971. The manuscript was submitted for publication on June 9, 1971.

The authors wish to thank John P. Decker of NASA-Langley for providing the wind tunnel models.

This technical report has been reviewed and is approved.

Emmett A. Niblack, Jr.
Lt Colonel, USAF
AF Representative, VKF
Directorate of Test

Joseph R. Henry
Colonel, USAF
Director of Test

ABSTRACT

Wind tunnel tests were conducted to determine the dynamic- and static-stability derivatives of an approximately 0.011-scale North American Rockwell straight wing and delta wing orbiters in proximity with an 0.011-scale General Dynamics/Convair delta wing booster. Interference-free data on the orbiter models were also obtained. Measurements were made with a forced-oscillation dynamic balance as the model oscillated ±1.6 deg at angles of attack ranging from -6.8 to 9.7 deg. Data were obtained at Mach numbers 1.76 and 2 and at free-stream Reynolds numbers, based on orbiter model length, ranging from 2.03×10^6 to 6.33×10^6. Both orbiter configurations were dynamically and statically stable, and in general, the level and trends of the orbiter derivatives were not greatly affected when in the proximity of the booster. The present damping data show fair agreement with damping data from the National Aeronautical Establishment (NAE), which are the only other known damping data of this type. However, the absolute level of the NAE C_{m_α} data, which were obtained using the half-model technique, was approximately 50 percent lower than that of the present data obtained on a three-dimensional model. Some disagreement was also found between the present static-stability data and data from the NASA-Ames and NASA-Langley test facilities.

CONTENTS

APPENDIXES

I. ILLUSTRATIONS

Figure

NOMENCLATURE

C_m	Pitching-moment coefficient, pitching moment/$q_\infty S_W \bar{c}$
C_{m_α}	$\partial C_m/\partial\alpha$, 1/radian
$C_{m_{\dot\alpha}}$	$\partial C_m/\partial(\dot\alpha\bar{c}/2V_\infty)$ } Local damping-in-pitch derivatives,
C_{m_q}	$\partial C_m/\partial(q\bar{c}/2V_\infty)$ } 1/radian
C_N	Normal-force coefficient, normal force/$q_\infty S_W$
C_{N_α}	$\partial C_N/\partial\alpha$, 1/radian
$\bar{c}$	Mean aerodynamic chord (reference length), ft
L	Booster model length, ft or in.
ℓ	Orbiter model length, ft or in.
M_∞	Free-stream Mach number
p_o	Tunnel stilling chamber pressure, psia
q	Pitching velocity, radians/sec
q_∞	Free-stream dynamic pressure, psia
Re_ℓ	Free-stream Reynolds number based on model length
S_W	Reference area (total wing area), ft^2 or $in.^2$
T_o	Tunnel stilling chamber temperature, °R
V_∞	Free-stream velocity, ft/sec
X	Longitudinal separation distance between booster and orbiter center of gravity, in.
x_{cg}	Distance from model nose to center of gravity (pivot axis), in.
Z	Vertical separation distance between booster and orbiter center of gravity, in.
α	Angle of attack, deg
α_{trim}	Trim angle of attack, deg
$\dot\alpha$	Time rate of change of angle of attack, radian/sec
δ_e	Elevator angle, deg
θ	Oscillation amplitude, deg
ω	Angular frequency, radian/sec
$\omega\bar{c}/2V_\infty$	Reduced frequency parameter, radian

SECTION I
INTRODUCTION

The problem of abort separation of the space shuttle vehicle is really not a new problem. Separation studies of two parallel lifting stages were initiated during the 1959-1960 Air Force reusable booster studies. In 1962, Langley Research Center started its investigation of the abort separation problem. John P. Decker of NASA Langley authored several papers and technical reports concerning abort separation characteristics of reusable launch vehicles. The majority of these reports are referenced in Ref. 1. It became apparent from this early work that in order to provide meaningful information on the magnitude and character of the separation problem it was necessary to determine the behavior of the vehicles during the staging maneuver. Langley developed a two-body trajectory simulation computer program which utilized static aerodynamic data. Results from this program showed that staging should occur outside the sensible atmosphere, and current space shuttle vehicles are designed for normal separation outside the sensible atmosphere. It is possible that the mission may have to be aborted before the design separation occurs; therefore, the vehicles must have the capability of performing the separation maneuver safely.

Decker (Ref. 1), utilizing the two-body trajectory program, showed that current estimated interference-free values of the pitch damping dynamic-stability derivatives are one or more orders of magnitude smaller than the values needed to achieve safe operation. In order to increase the damping-in-pitch derivatives by using stability augmentation, one must know accurate interference-free damping values, and also how the damping derivatives vary when the two vehicles are in proximity to each other.

To date, almost all the experimental separation tests have been concerned with obtaining static-stability data. It is evident that the damping derivatives of two vehicles when in proximity to each other must also be measured. Orlik-Ruckemann of NAE has obtained limited dynamic-stability data on a space shuttle vehicle utilizing the half-model technique (Ref. 2). The purpose of the present test program is to obtain pitch damping dynamic-stability data on a complete 3-dimensional vehicle when in close proximity with another vehicle.

The present tests were conducted in the von Kármán Gas Dynamics Facility (VKF), Supersonic Wind Tunnel (A), on an approximately 0.011-scale North American Rockwell straight wing and delta wing orbiters with and without an 0.011-scale General Dynamics/Convair

delta wing booster in proximity. Data were obtained at Mach numbers 1.76 and 2 at Reynolds numbers, based on model length, of 2.03×10^6 to 6.33×10^6. A small-amplitude forced-oscillation balance was used to obtain data at oscillation amplitudes of approximately ±1.6 deg at angles of attack from -6.8 to 9.7 deg.

SECTION II
APPARATUS

2.1 TEST FACILITY

The Supersonic Wind Tunnel (A) (Fig. 1, Appendix I) is a continuous, closed-circuit, variable density wind tunnel with an automatically driven flexible-plate-type nozzle and a 40- by 40-in. test section. The tunnel can be operated at Mach numbers from 1.5 to 6 at maximum stagnation pressures from 29 to 200 psia, respectively, and at stagnation temperatures up to 750°R. Minimum stagnation pressures range from about one-tenth to one-twentieth of the maximum pressures at each Mach number. Mach number changes may be made without stopping the tunnel in most instances. The orbiter model could be injected into the tunnel for a test run and then retracted for model changes without interrupting the tunnel flow.

2.2 MODELS

The models tested were approximately 0.011 scale and were fabricated at NASA-Langley Research Center. The North American Rockwell straight wing (NARSW) orbiter (Fig. 2a) is known as the 130C configuration with the 130G wing location, and the North American Rockwell delta wing (NARDW) orbiter (Fig. 2b) is known as the 134D configuration. The delta wing booster is an approximate General Dynamics/Convair B9U booster without canards or vertical tail. The two orbiter models, fabricated from aluminum, were tested alone and in proximity with the delta wing booster. The straight wing orbiter, typical of a low cross range orbiter, had a leading-edge sweep of 21.6 deg. The delta wing orbiter, typical of a high cross range orbiter, had a leading edge sweep of 60 deg. The delta wing orbiter was tested with elevator deflections of 0 and -20 deg. The fuselage of the delta wing booster was constructed from mahogany, and the delta wing, with a leading-edge sweep of 52.5 deg, was fabricated from aluminum. Model geometries are shown in Fig. 3.

The orbiter model was sting supported to the tunnel pitch mechanism, and the booster model was supported from the top of the tunnel by a vertical strut. A photograph and a sketch of the model installation are shown in Figs. 4 and 5, respectively.

2.3 INSTRUMENTATION

The small amplitude (±3 deg) forced-oscillation balance system (Ref. 3) is a one-degree-of-freedom oscillatory system incorporating a cross-flexure pivot. During the test, model oscillation amplitudes were approximately ±1.6 deg. The balance is forced to oscillate by an electromagnetic shaker motor located in the aft portion of the sting. The angular displacement of the model is measured by a strain-gage bridge mounted on a cross flexure, and the input torque to the system is measured by a strain-gage bridge mounted at the minimum cross-sectional area of the torque beam. Whenever the model balance system was oscillated at a frequency other than its undamped natural frequency, electronic resolvers were used to determine the in-phase and out-of-phase components of the forcing torque signal. The forcing system is equipped with a feedback control network as described in Ref. 3 to provide positive amplitude control for testing either dynamically stable or unstable configurations.

SECTION III
PROCEDURE

3.1 TEST PROCEDURE

The orbiter model was oscillated at oscillation amplitudes of approximately ±1.6 deg, and the resulting time-resolved torque signal, in-phase and out-of-phase components of the torque signal, and displacement signal were recorded on magnetic tape by a high-speed digital converter and relayed to the computer for data reduction. The method used for reducing the data may be found in Ref. 3.

The orbiter models were tested alone and in proximity with the booster model to obtain interference-free and interference data, respectively. The orbiter model could traverse in the longitudinal direction, and the booster model was movable in the vertical plane of the tunnel. For a given orbiter longitudinal position (X/L) relative to the booster model which was at a pre-determined separation distance (Z/L) relative to the orbiter model, the orbiter model was pitched to discrete angles of attack, and damping data were obtained.

A matrix of test conditions is shown in Fig. 6, and a test summary of model configurations and wind tunnel test conditions is presented in Tables I and II (Appendix II), respectively.

3.2 DATA PRECISION

The balance was calibrated before and after the tests, and check calibrations were made before and after each run. In addition, structural damping values were obtained at vacuum conditions before the tunnel entry to evaluate the still-air damping contribution.

The estimated uncertainty of the dynamic- and static-stability derivatives using an analysis presented in Ref. 4 is as follows:

For the straight wing orbiter,

		Uncertainty	
M_∞	$Re_\ell \times 10^{-6}$	ΔCm_α	$\Delta(Cm_q + Cm_{\dot\alpha})$
1.76, 2.00	1.95	±0.068	±0.87
1.76	4.23	±0.053	±0.99
1.76	6.33	±0.049	±1.07

For the delta wing orbiter,

M_∞	$Re_\ell \times 10^{-6}$	ΔCm_α	$\Delta(Cm_q + Cm_{\dot\alpha})$
2.00	1.95, 4.08	±0.02	±0.11

SECTION IV
RESULTS AND DISCUSSION

Figures 7 and 8 show the comparison of the interference data (orbiter in proximity with the booster) and the interference-free data (orbiter alone) for the straight wing orbiter at $M_\infty = 2$. For the separation parameters (X/L, Z/L) investigated, the interference derivatives show approximately the same levels as the interference-free derivatives. The dynamic and static derivatives also show no large variation with angle of attack (Fig. 8).

Figures 7 and 8 also show Orlik-Ruckemann's dynamic stability data that were obtained at the National Aeronautical Establishment (NAE) at $M_\infty = 1.8$ using the half-model technique. The NAE orbiter and booster were 0.00278-scale straight wing models. The NAE Cm_α data were transferred to the present center-of-gravity position

(x_{cg}/ℓ = 0.601) using a value for C_{N_α} of 3.44 per radian. The NAE damping data generally show fair agreement with the present damping data (Figs. 7a and 8). However, the NAE static stability data show the configuration to be substantially less stable than the present data. This disagreement will be further discussed in a later paragraph where the data comparison is at essentially the same Mach number.

Additional comparisons (Refs. 5 and 6) of the interference-free static-stability derivatives for the straight wing orbiter are shown in Fig. 9. The NASA-Ames and -Langley data trends are similar to the present data trends, but for the positive angles of attack, the absolute levels of the NASA data are higher than the present data.

The effect of Reynolds number on the interference-free dynamic derivatives for the straight-wing orbiter at M_∞ = 1.76 is shown in Figs. 10 and 11. The damping-in-pitch derivatives at an average angle of attack of approximately 0.6 deg and at α_{trim} increased slightly with increasing Reynolds number (Fig. 10). The static-stability derivatives were essentially invariant with Reynolds number (Fig. 10). In Fig. 11, the dynamic derivatives show no large gradients for the angle-of-attack range of -2 to 6 deg for the Reynolds numbers investigated. In general, the damping derivatives increased with Reynolds numbers for the angle-of-attack range investigated. The static-stability derivatives (Fig. 11) decreased with increasing angle of attack and were not a function of Reynolds number. With Mach number and Reynolds number essentially matched, the NAE damping data at α = 0 compare favorably with the present data (Fig. 11). However, the absolute level of the NAE C_{m_α} data was approximately 50 percent lower than the present data. The NAE data were obtained using the half-model test technique, whereas the present data were obtained on a 3-dimensional model.

Figure 12 shows the effect of oscillation amplitude on the interference-free dynamic- and static-stability derivatives at M_∞ = 1.76 for $Re_\ell \approx 6.4 \times 10^6$. Increasing the oscillation amplitude from ±1 to ±1.6 deg increased model damping but had no effect on the static-stability derivatives. Typical interference and interference-free schlieren photographs for the straight wing shuttle configuration are shown in Fig. 13.

The interference and interference-free dynamic- and static-stability derivatives as a function of angle of attack are shown in Fig. 14 for various positions of the delta wing orbiter relative to the delta wing booster. The interference and interference-free dynamic- and static-stability derivatives were essentially invariant with angle of attack.

The delta wing orbiter data are shown in Figs. 15 and 16 as a function of X/L for Z/L ≈ 0.15 and 0.35, respectively. The dynamic- and static-stability derivatives show no large variation with relative longitudinal position of the orbiter to the booster, and the derivatives are about the same level as the interference-free data. It is interesting to note that, at X/L ≈ -0.1, Z/L ≈ 0.15 (Fig. 15), model damping is a minimum at α = 0 and ±2 deg compared with the other X/L positions. At α = 4 deg, model damping is invariant with X/L. By referring to the schlieren photographs (Fig. 17b) for these test conditions, the orbiter nose at α = 4 deg is much closer, or within the booster bow shock, than at α = 0 and -4 deg.

Figures 18 and 19 show the effect of the vertical separation distance (Z/L) on the damping and static derivatives for X/L ≈ 0.02 and -0.31, respectively. Model damping and static stability generally decreased as Z/L was increased. An exception to this was at α = -4, X/L ≈ 0.02, where the static stability increased (Fig. 18b). The level of the interference-free data generally was between the level of the interference data at Z/L ≈ 0.15 and 0.35.

Results of a modest investigation of Reynolds number effect on the delta wing interference data are shown in Figs. 20 and 21. For $Re_{\ell} \approx 2 \times 10^6$ and 4×10^6, the levels and trends of the dynamic- and static-stability derivatives are approximately the same.

The effect of elevator angle on the delta wing orbiter at M_∞ = 2 is shown in Fig. 22. Model damping was not affected by the elevator angle. Changing the δ_e from 0 to -20 increased the trim angle from 1.5 to 4.8 deg, respectively, and also increased the static stability.

SECTION V
CONCLUSIONS

Wind tunnel tests were conducted to obtain dynamic-stability data on a three-dimensional vehicle when in close proximity with another vehicle. Data were obtained at Mach numbers 1.76 and 2.00 at Reynolds numbers (based on orbiter model length) of 2.03×10^6 to 6.33×10^6. Conclusions based on the results presented in this report are given below:

1. For the present test conditions and configurations, the orbiter dynamic- and static-stability derivatives were not greatly affected when the orbiter vehicle was in close proximity with the booster vehicle.

2. For the interference-free delta wing configuration at $M_\infty = 2.00$, $Re_\ell \approx 2 \times 10^6$, the dynamic- and static-stability derivatives were essentially invariant with angle of attack.

SECTION VI
FURTHER POSSIBLE DEVELOPMENTS

The limited AEDC and NAE test results showed no striking effects of the proximity of the booster on the pitch dynamic stability of the orbiter. However, one must not conclude that an abort dynamic-stability problem does not exist. These tests were conducted at essentially one Mach number and one Reynolds number, while the abort condition could be at any one of several Mach number and Reynolds number combinations. The effect of the following additional parameters should also be investigated: Mach number, wider range of Reynolds numbers, center-of-gravity location, reduced frequency parameter, and amplitude of oscillation with either one or both vehicles oscillating. In addition, the damping derivatives could be configuration dependent.

The test technique used for the present test can also be used in the Mach 8 and 10 wind tunnels at the AEDC von Kármán Gas Dynamic Facility (VKF). With some modification, there is also the possibility that the present technique could be used in the AEDC Propulsion Wind Tunnel Facility (PWT) for testing at subsonic and transonic Mach numbers.

REFERENCES

1. Decker, John P., McGhee, Robert J., and Pierpont, P. Kenneth. "Abort Separation Including Aerodynamic, Dynamic, Propulsive, and Trajectory Influences." Space Transportation System Technology Symposium, NASA TM X-52876, Vol. I, July 1970.

2. Orlik-Ruckemann, K. J., and LaBerge, J. G. "Dynamic Stability Experiments on Straight Wing Space Shuttle Abort Separation at M = 1.80." National Research Council of Canada. NAE LTR-UA-16, May 1971.

3. Schueler, C. J., Ward, L. K., and Hodapp, A. E., Jr. "Techniques for Measurements of Dynamic Stability Derivatives in Ground Test Facilities." AGARDograph 121 (AD669227), October 1967.

4. Beers, Yardley. Introduction to the Theory of Error. Addison Wesley Publishing Company, Inc., Reading, Massachusetts, 1957, pp. 26-36.

5. Malcolm, Gerald N. "Aerodynamic Characteristics of Space Shuttle Vehicles-North American Rockwell Orbiters." SADSAC/Space Shuttle Wind Tunnel Test Data Report. NASA Ames Research Center. DMS-DR-1026, October 1970.

6. Powell, R. W. "Stability and Control Investigation of NAR Straight Wing Orbiter (M = 1.5 to 2.0)." SADSAC/Space Shuttle Wind Tunnel Test Data Report. NASA Langley Research Center DMS-DR-1069, March 1971.

APPENDIXES
I. ILLUSTRATIONS
II. TABLES

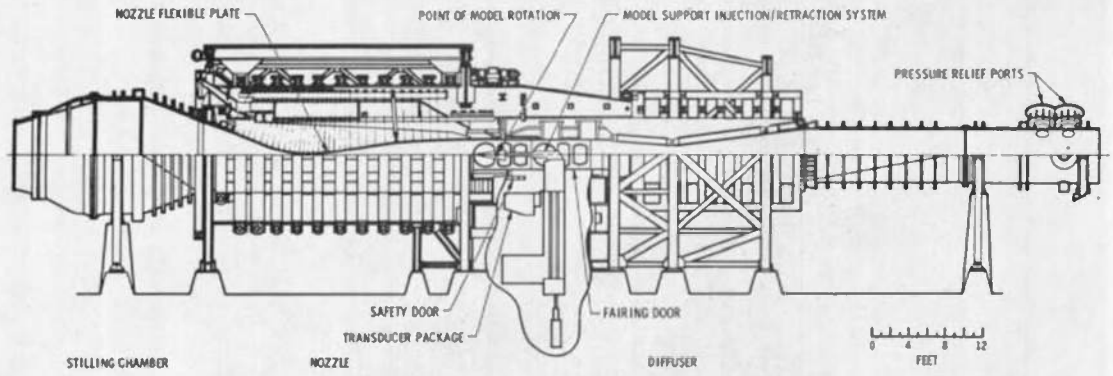

a. Tunnel A Assembly

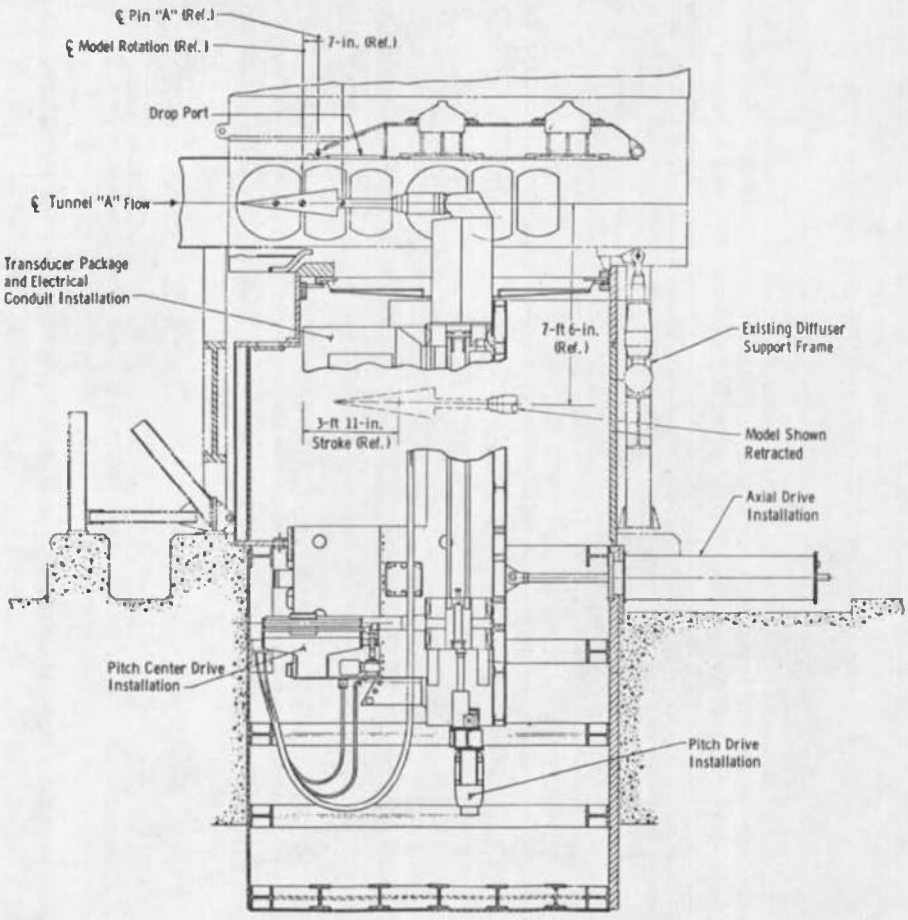

b. Tunnel A Model Injection System

Fig. 1 Tunnel A Details

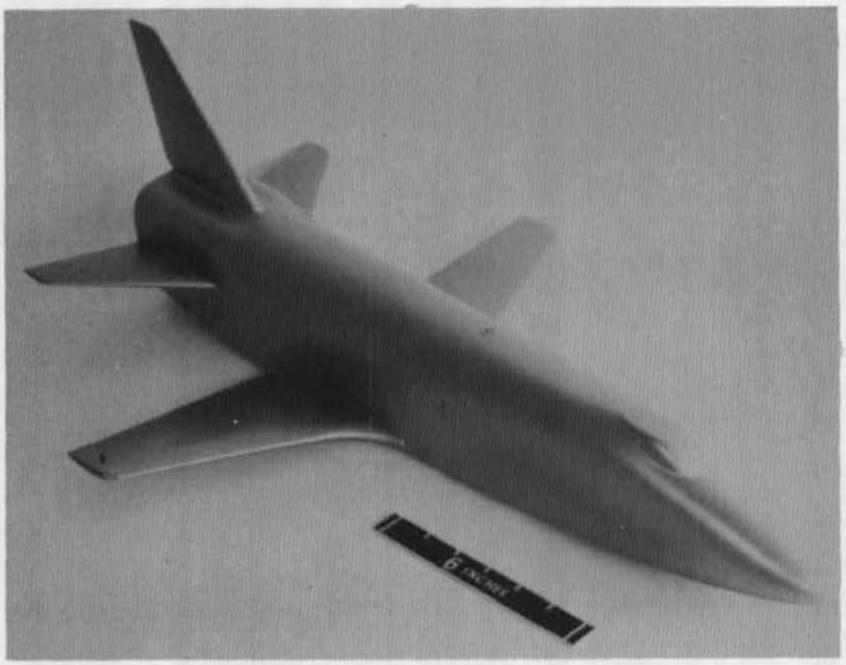

a. Straight Wing

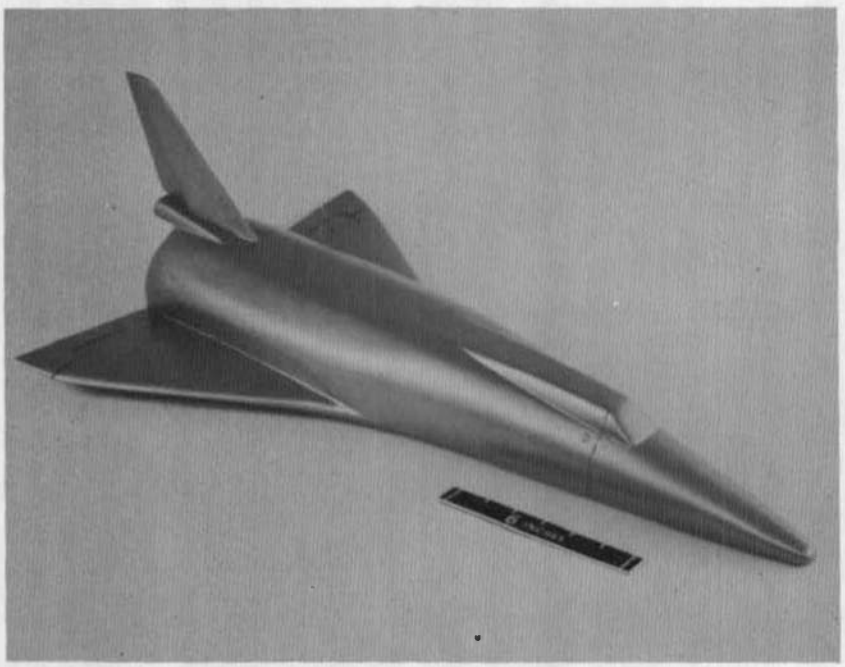

b. Delta Wing

Fig. 2 Photographs of Orbiter Models

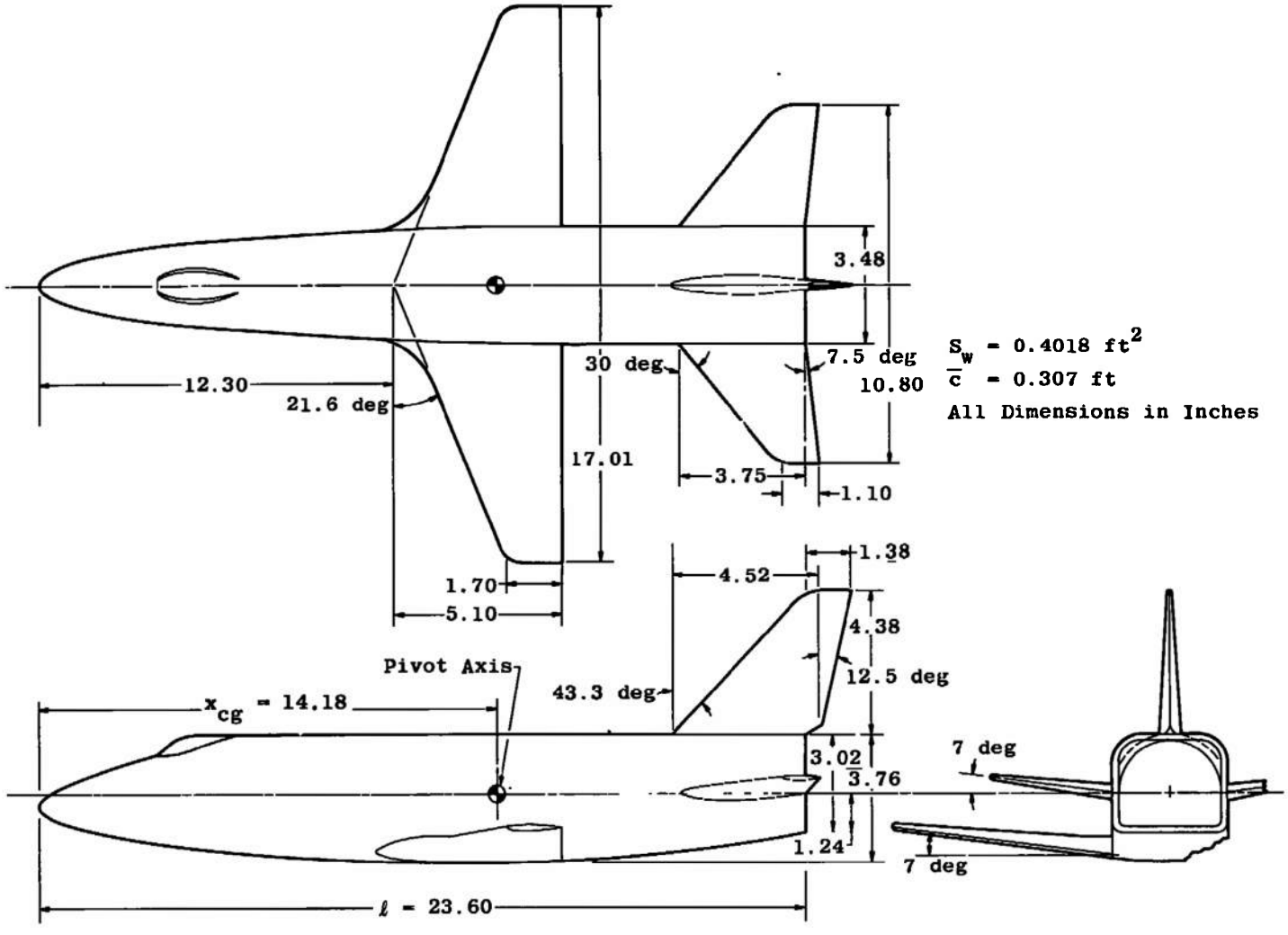

a. Straight Wing Orbiter

Fig. 3 Model Geometries

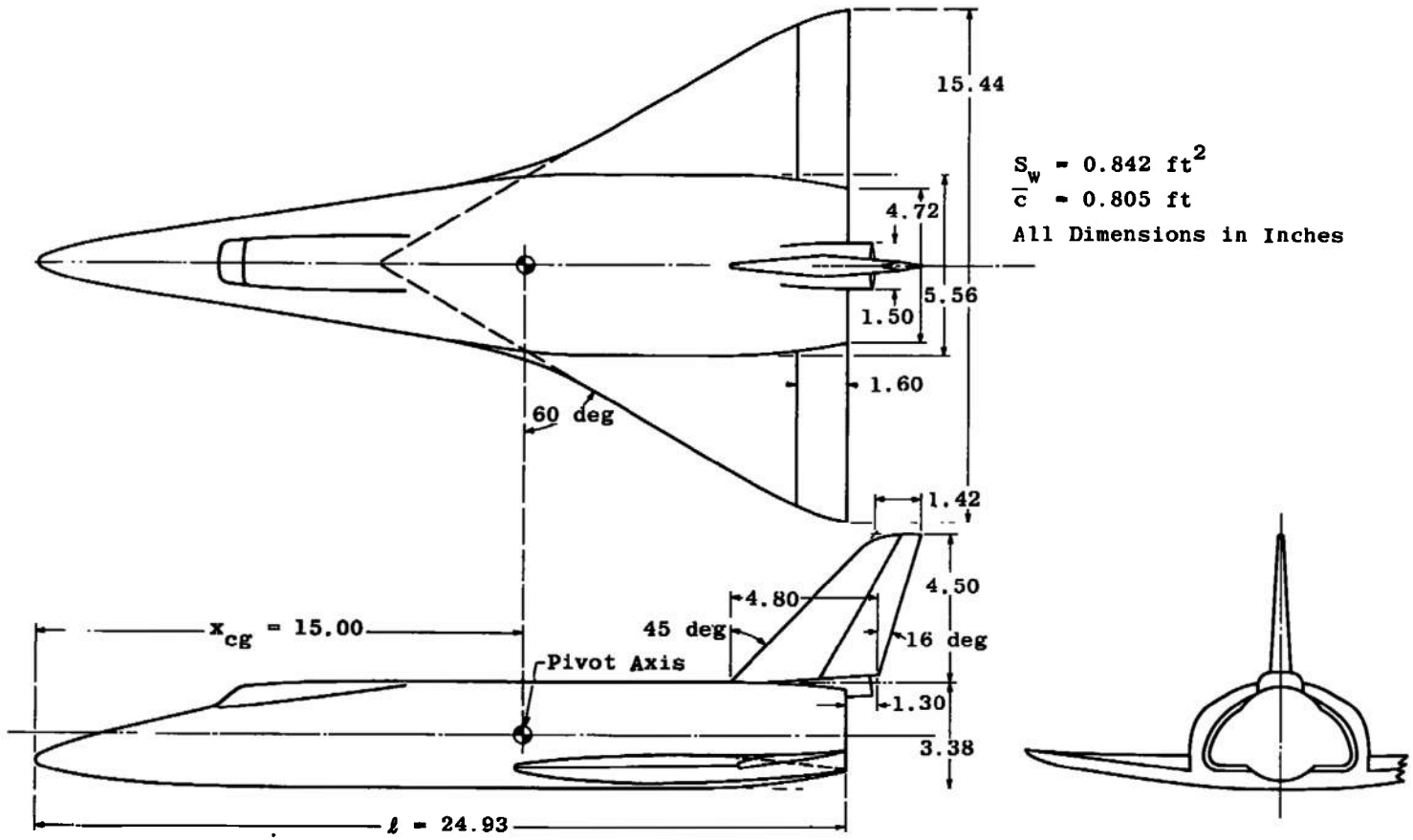

b. Delta Wing Orbiter
Fig. 3 Continued

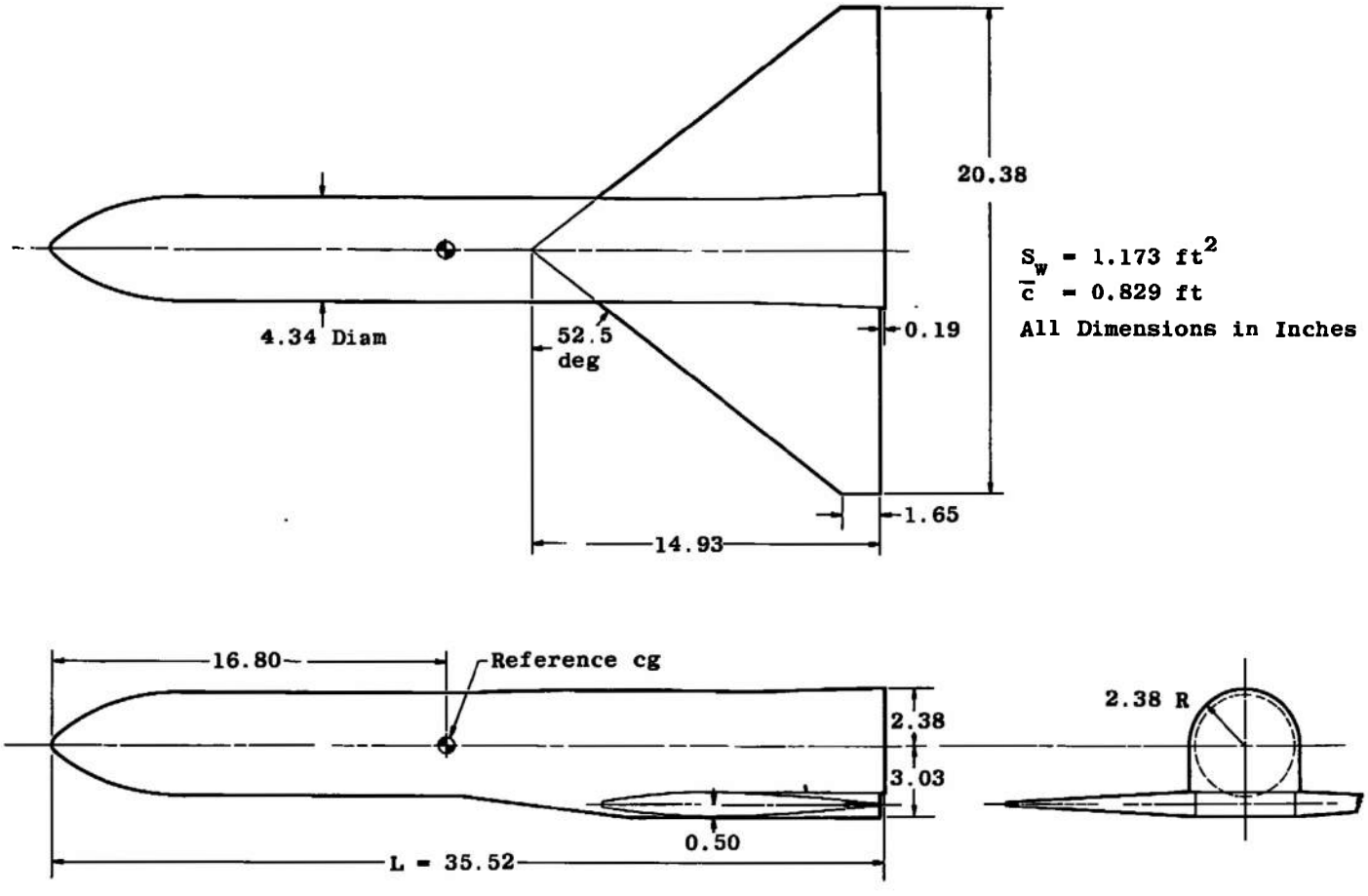

c. Delta Wing Booster
Fig. 3 Concluded

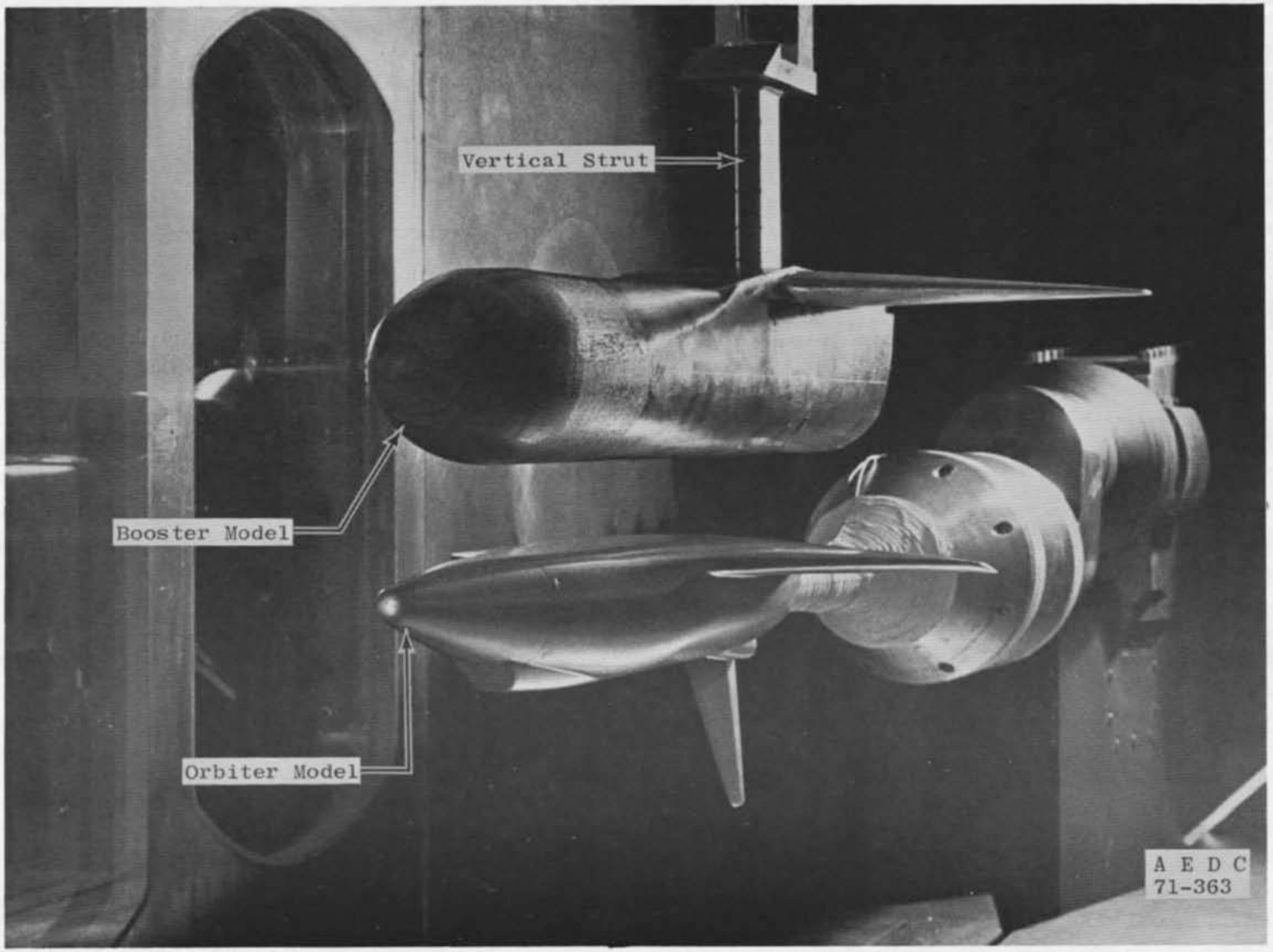

Fig. 4 Installation Photograph

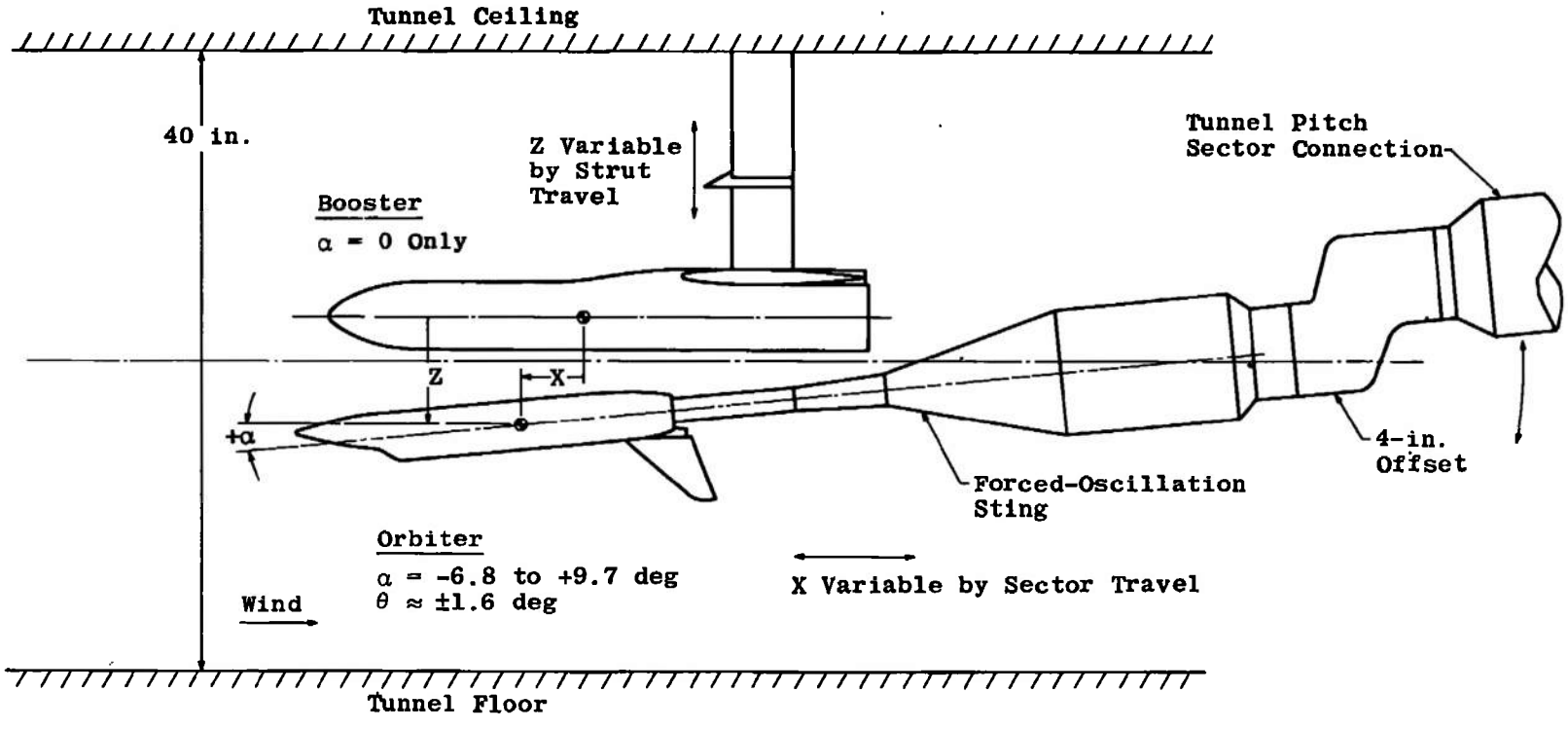

Fig. 5 Installation of Space Shuttle Models in Tunnel A for Dynamic-Stability Abort Separation Test (Models Inverted)

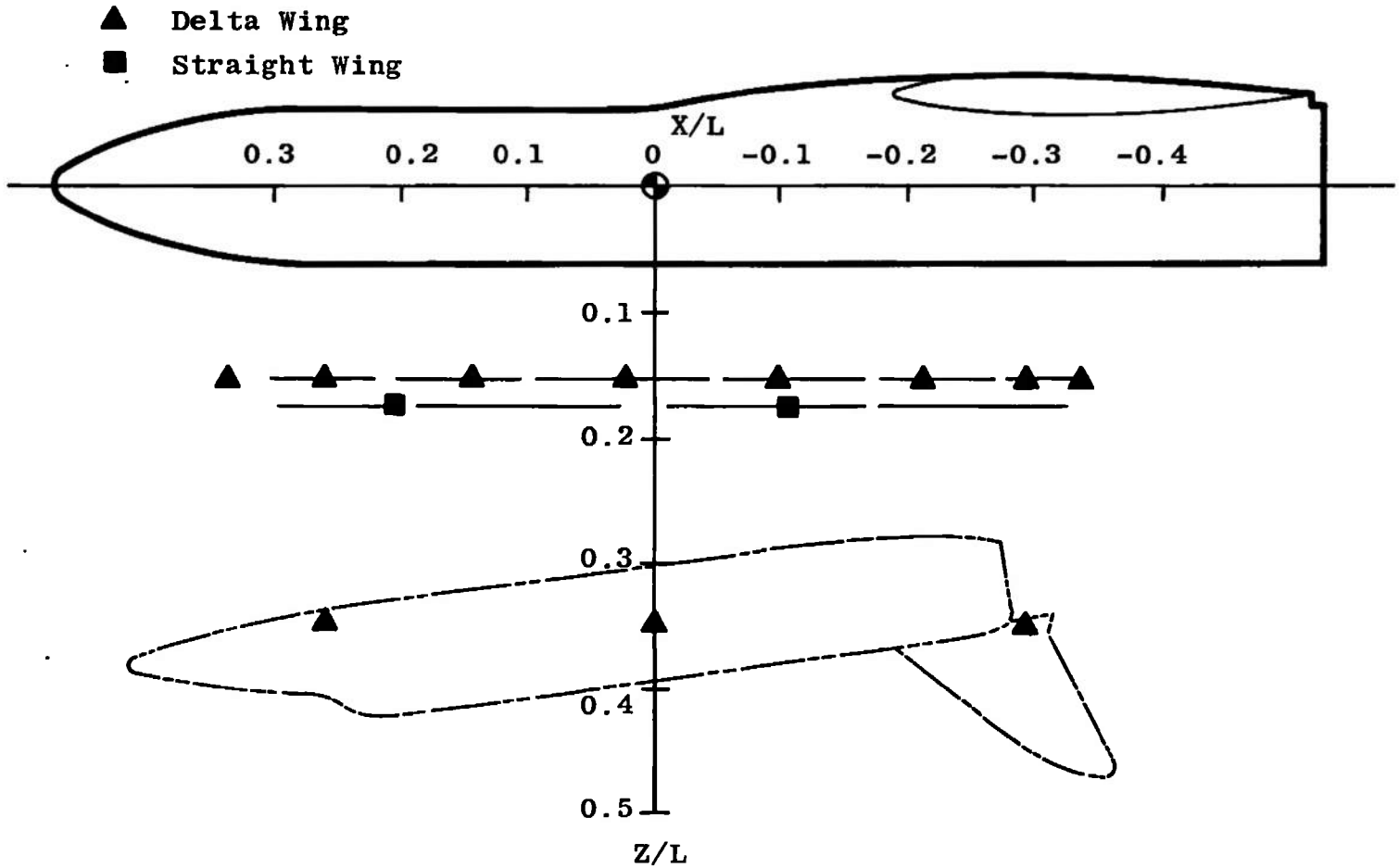

Fig. 6 Test Matrix Showing Orbiter CG Positions Relative to Booster CG for Data Taken

Sym	Facility	M_∞	$\approx Re_\ell \times 10^{-6}$	$\omega\bar{c}/2V_\infty$	x_{cg}/ℓ	Data
——	AEDC	2	2	0.0071	0.601	Interference Free
□	AEDC	2	2	0.0071	0.601	Interference
—·—	NAE (Ref. 2)	1.8	1.8	0.012	0.609	Interference Free
■	NAE (Ref. 2)	1.8	1.8	0.012	0.609	Interference

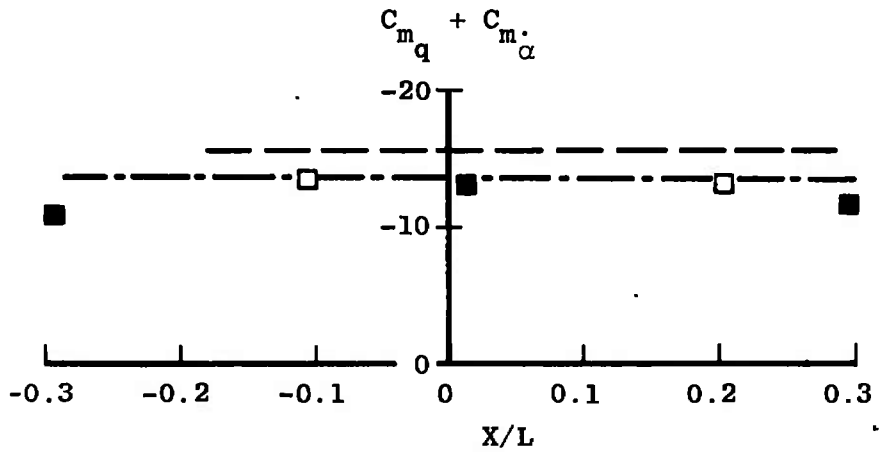

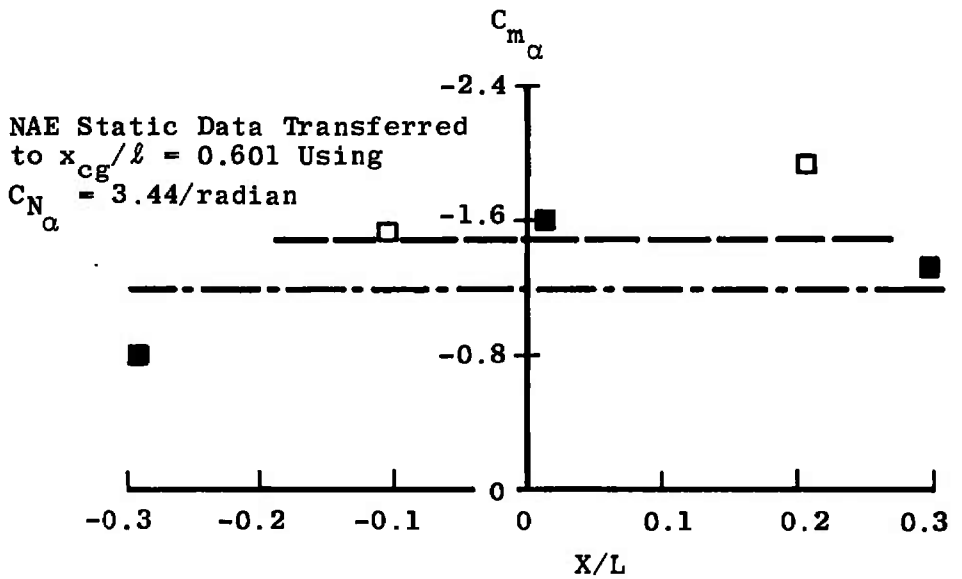

a. $\alpha = 0$

Fig. 7 Dynamic- and Static-Stability Derivatives as a Function of Relative Position of Orbiter and Booster, Straight Wing Orbiter and Delta Wing Booster, Z/L ≈ 0.17

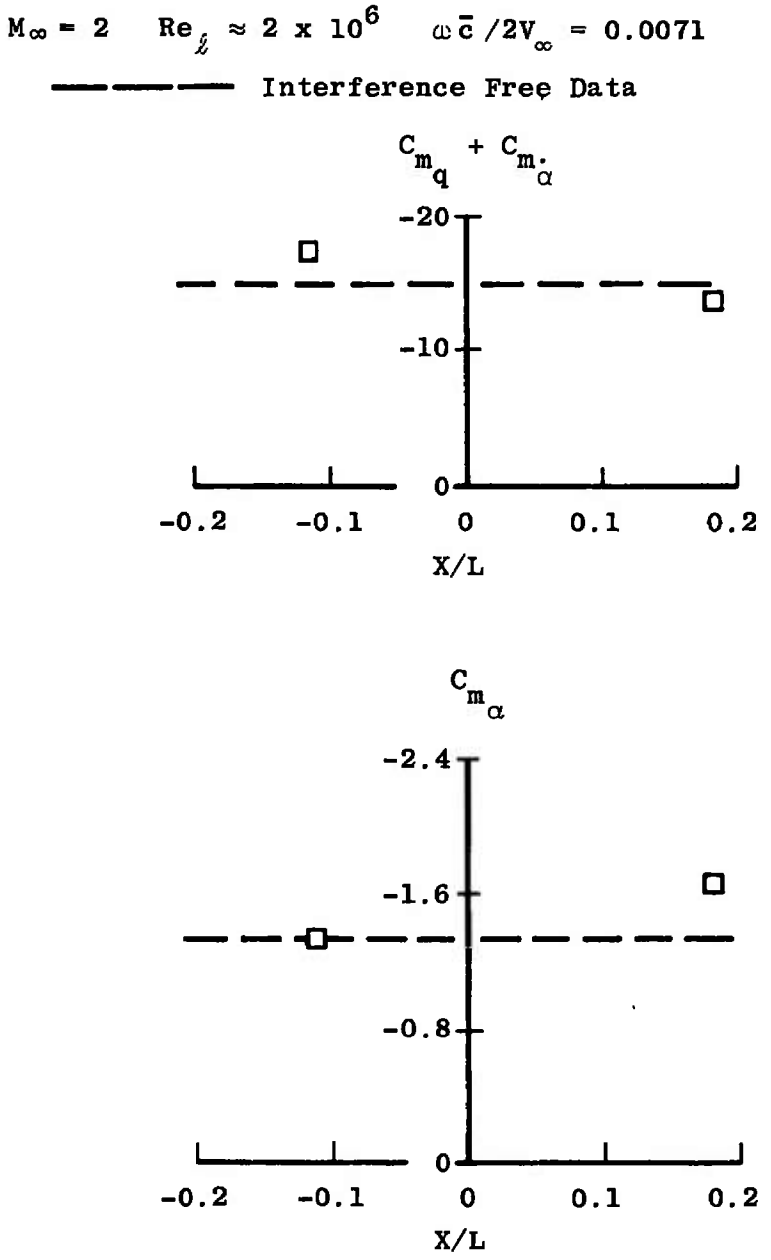

b. α = 5 deg

Fig. 7 Continued

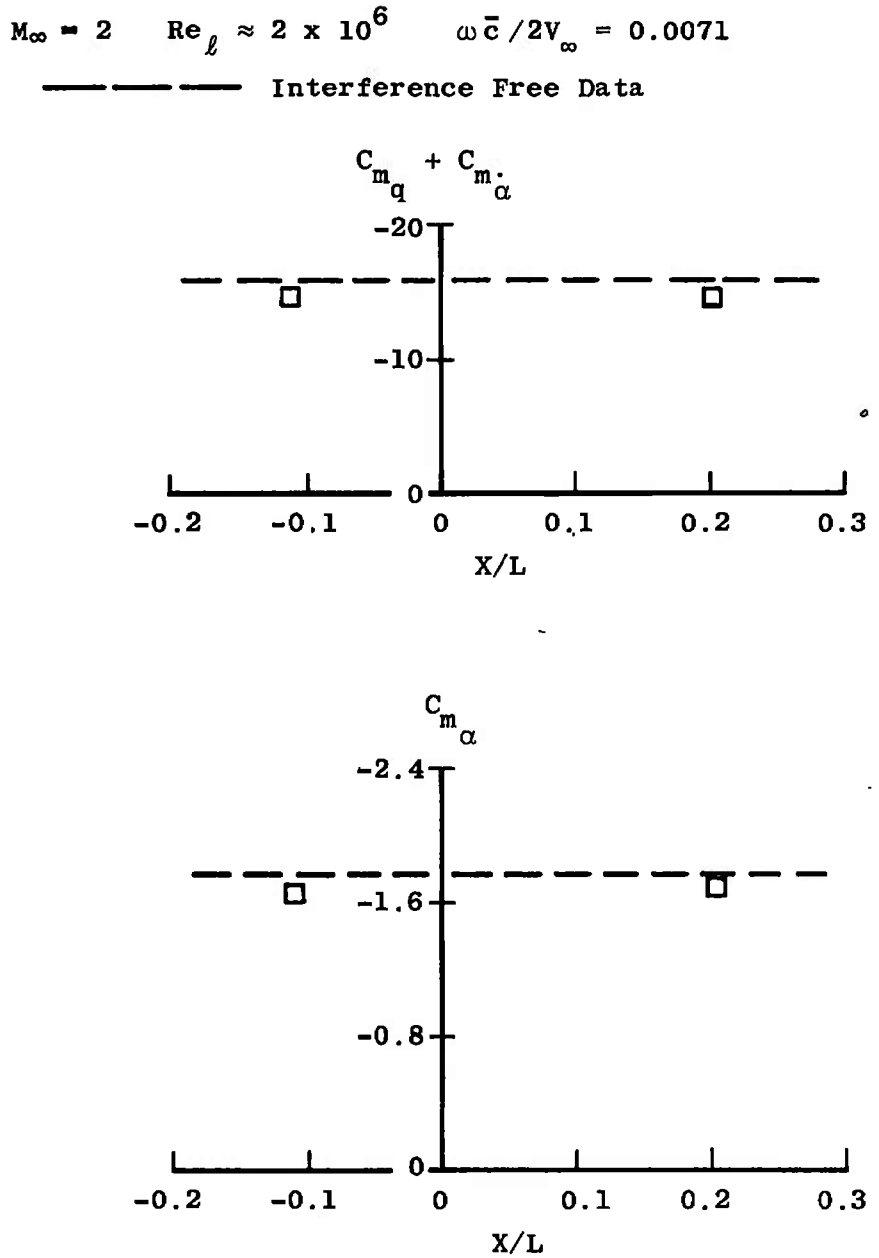

c. $\alpha = -4$ deg

Fig. 7 Concluded

Sym	Facility	M_∞	$\approx Re_\ell \times 10^{-6}$	$\omega \bar{c}/2V_\infty$	x_{cg}/ℓ	Data
○	AEDC	2	2	0.0071	0.601	Interference Free
□	AEDC	2	2	0.0071	0.601	Interference
●	NAE (Ref. 2)	1.8	1.8	0.012	0.609	Interference Free

Flagged Symbols - NAE Data Transferred to $x_{cg}/\ell = 0.601$ Using $C_{N_\alpha} = 3.44$/radian

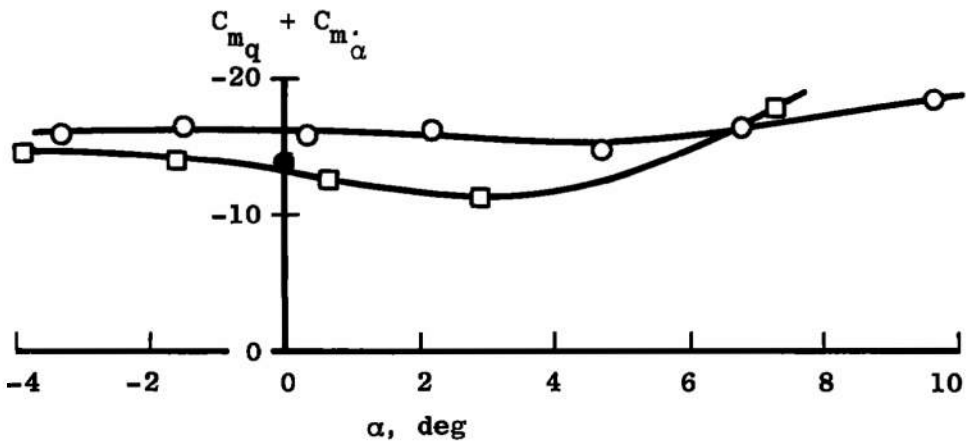

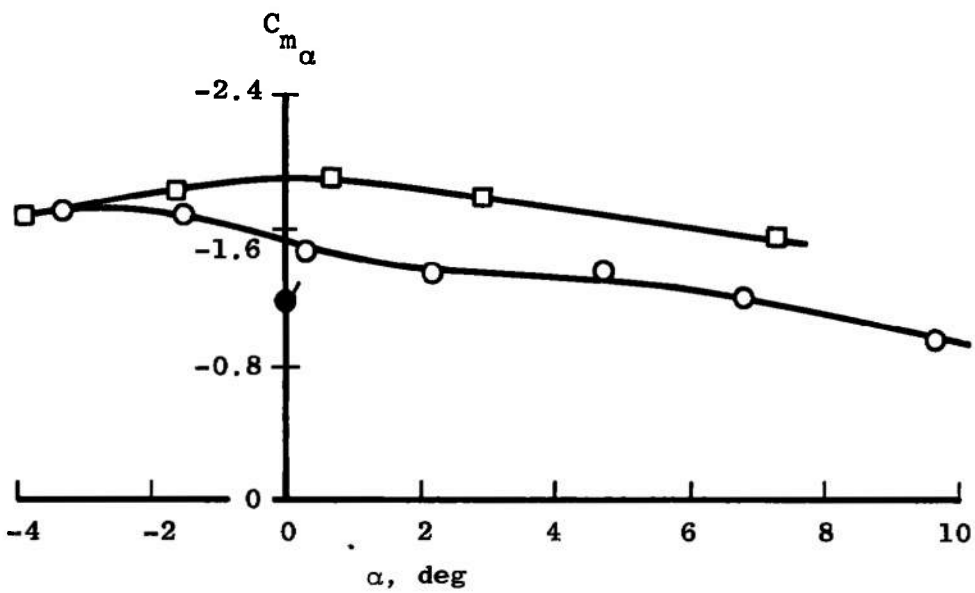

a. X/L ≈ 0.20, Z/L ≈ 0.17

Fig. 8 Dynamic- and Static-Stability Derivatives as a Function of Angle-of-Attack, Straight Wing Orbiter and Delta Wing Booster

Sym	Facility	M_∞	$\approx Re_\ell \times 10^{-6}$	$\omega \bar{c}/2V_\infty$	x_{cg}/ℓ	Data
○	AEDC	2	2	0.0071	0.601	Interference Free
□	AEDC	2	2	0.0071	0.601	Interference
●	NAE (Ref. 2)	1.8	1.8	0.012	0.609	Interference Free

Flagged Symbols - NAE Data Transferred to $x_{cg}/\ell = 0.601$ Using $C_{N_\alpha} = 3.44$/radian

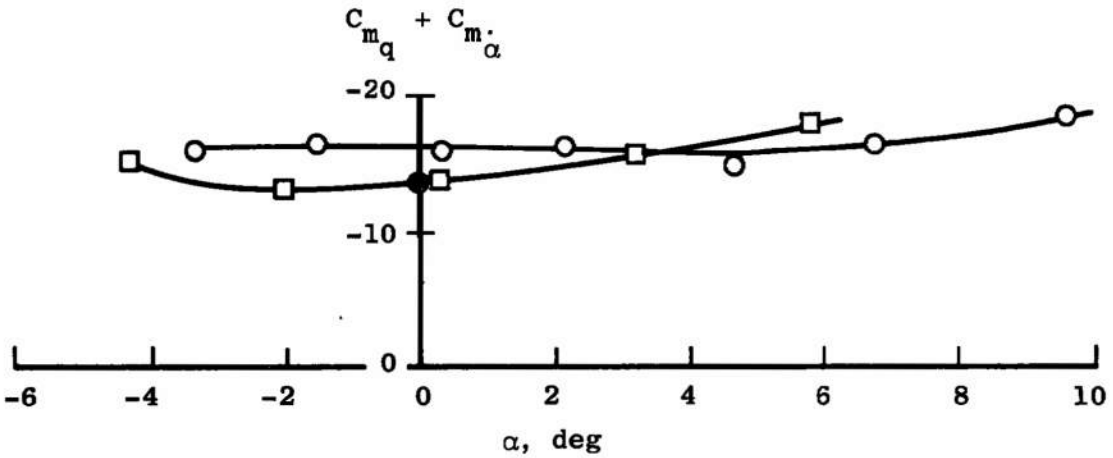

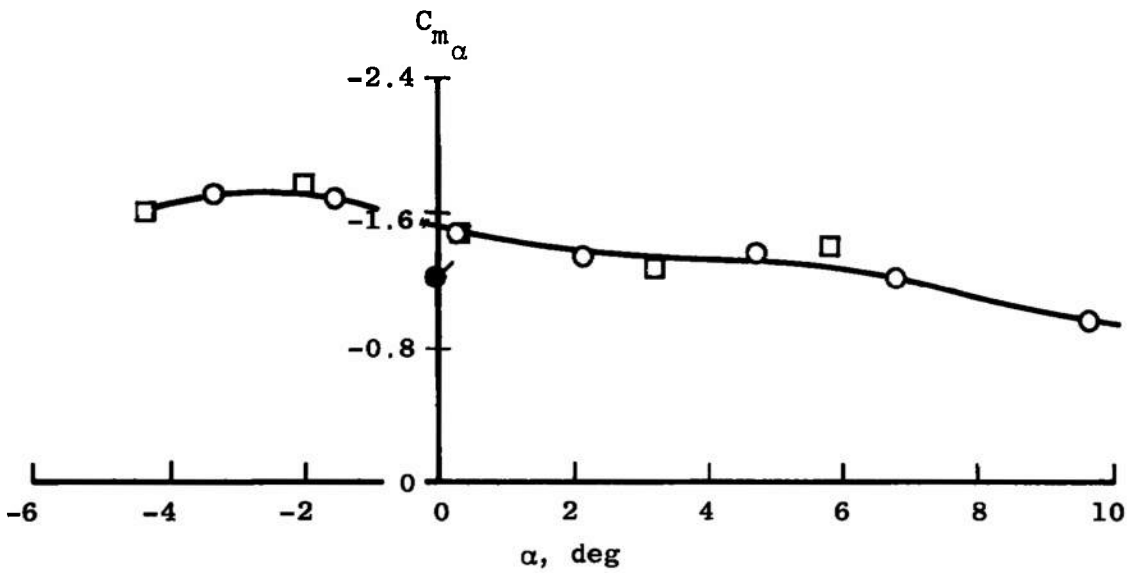

b. X/L ≈ -0.11, Z/L ≈ 0.17

Fig. 8 Concluded

Sym	Facility	M_∞	$\approx Re_\ell \times 10^{-6}$	x_{cg}/ℓ
○	AEDC	2.0	2.0	0.601
◺	NASA-Langley (Ref. 6)	2.0	1.0	0.601
△	NASA-Ames (Ref. 5)	2.0	3.3	0.601
●	NAE (Ref. 2)	1.8	1.8	0.601

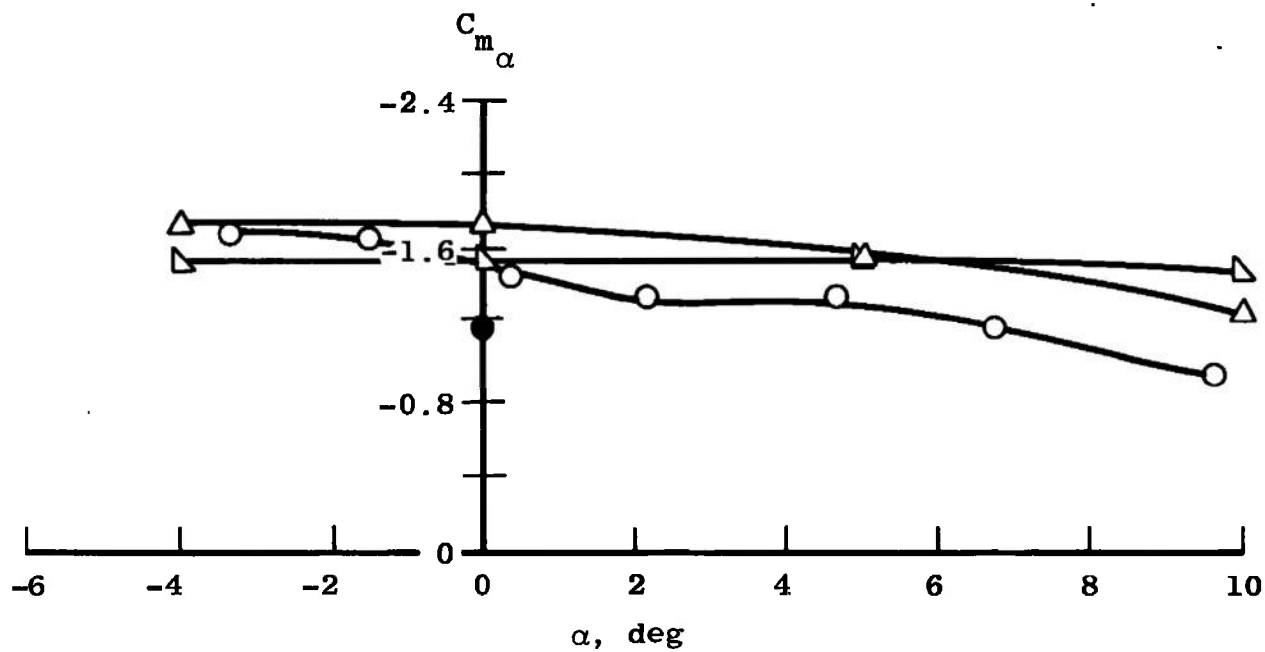

Fig. 9 Comparison of C_{m_α} Data Obtained from Static and Dynamic Tests, Straight Wing Orbiter, Interference Free

○ α, deg	□ α, deg	△ α, deg	$Re_\ell \times 10^{-6}$	$\omega \bar{c}/2V_\infty$
3.7	4.9	0.4	2.16	0.0076
3.5	4.8	0.7	4.23	0.0080
3.4	4.6	0.9	6.34	0.0083

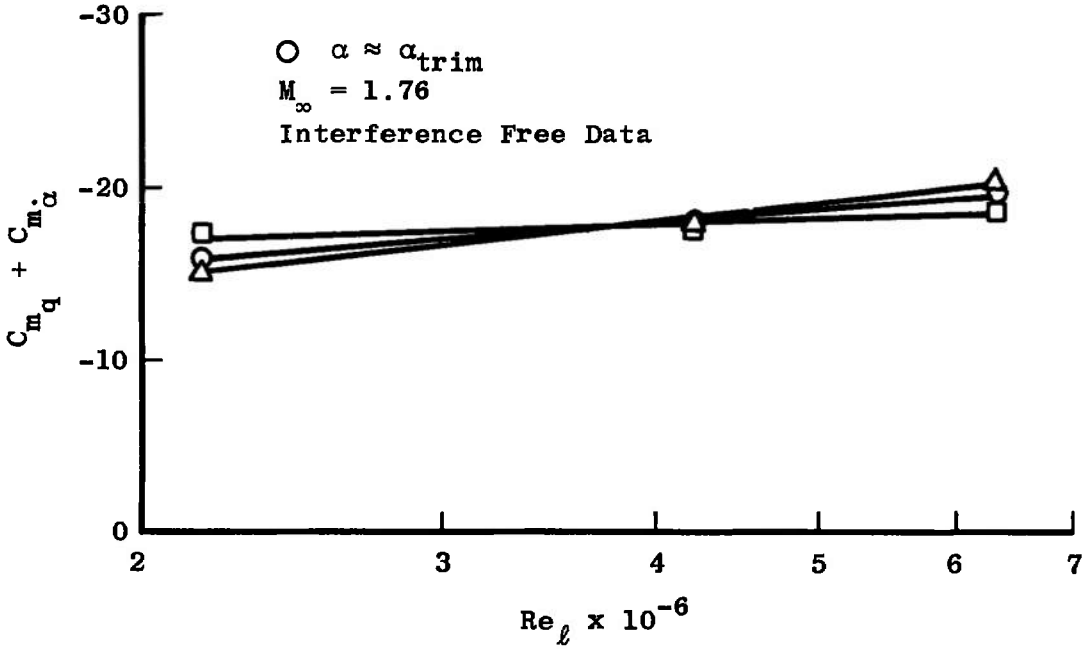

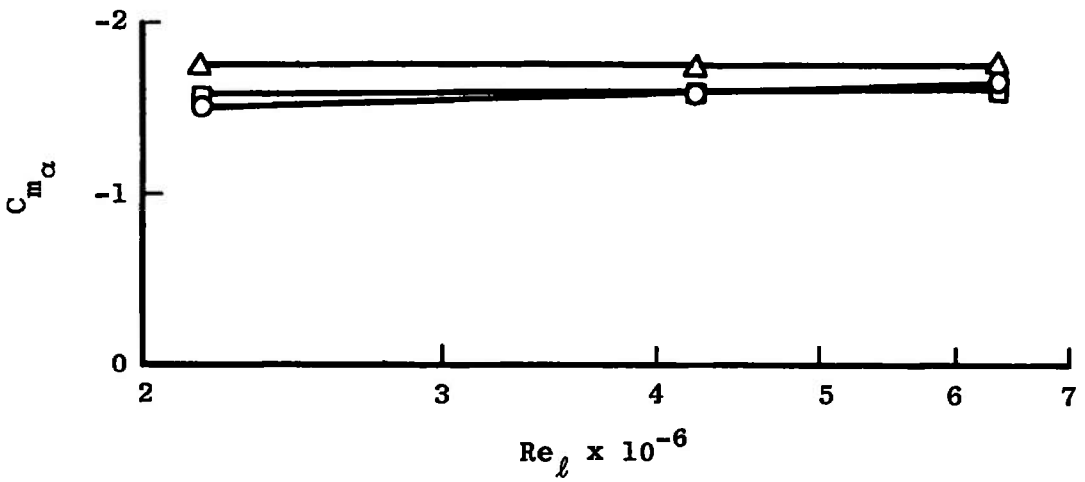

Fig. 10 Dynamic- and Static-Stability Derivatives as a Function of Reynolds Number for the Straight Wing Orbiter

Sym	Facility	M_∞	$\approx Re_\ell \times 10^{-6}$	$\omega \bar{c}/2V_\infty$	x_{cg}/ℓ
○	AEDC	1.76	2.1	0.0077	0.601
□	AEDC	1.76	4.2	0.0088	0.601
△	AEDC	1.76	6.4	0.0083	0.601
●	NAE (Ref. 2)	1.8	1.8	0.12	0.609

Flagged Symbols - NAE Data Transferred to $x_{cg}/\ell = 0.601$ Using $C_{N_\alpha} = 3.44$/radian

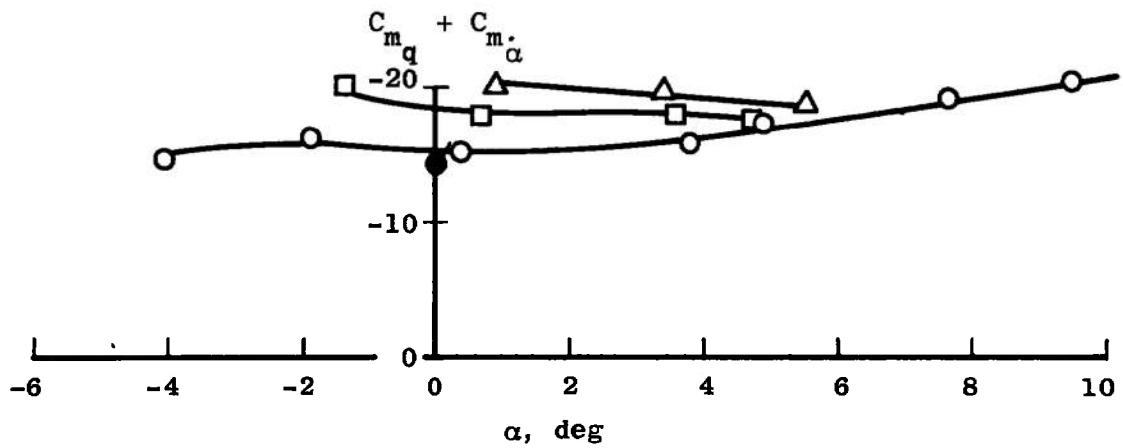

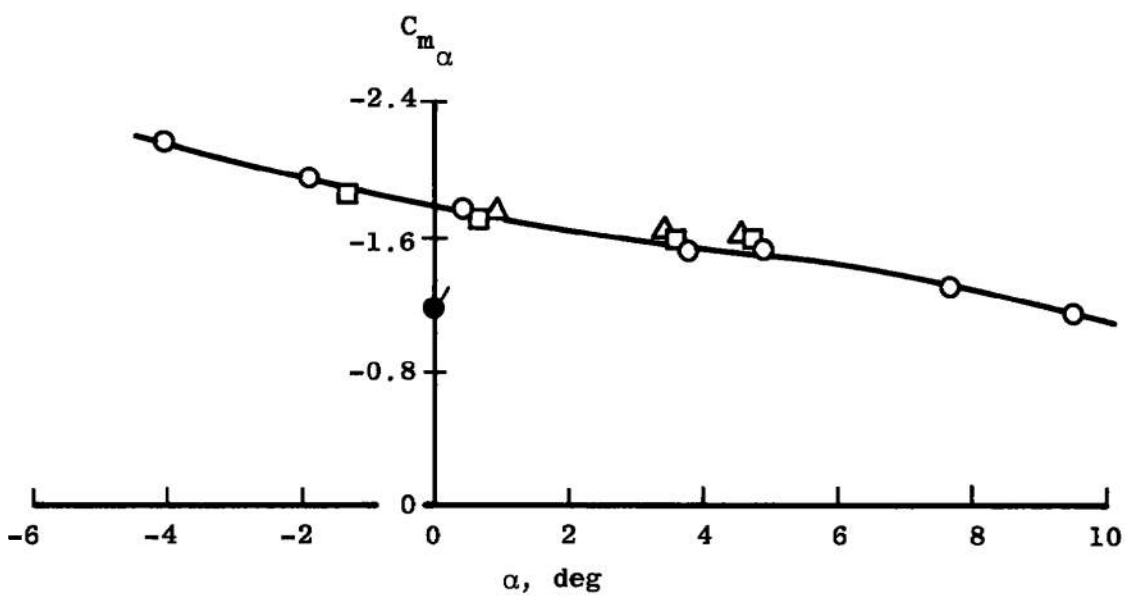

Fig. 11 Effect of Reynolds Number on Straight Wing Orbiter, Interference-Free Data

Sym	Facility	M_∞	$\approx Re_\ell \times 10^{-6}$	$\omega \bar{c}/2V_\infty$	x_{cg}/ℓ	$\pm\theta$, deg
○	AEDC	1.76	6.4	0.0083	0.601	1.6
□	AEDC	1.76	6.4	0.0083	0.601	1.0
●	NAE. (Ref. 2)	1.8	1.8	0.012	0.609	1.5

Flagged Symbols - NAE Data Transferred to $x_{cg}/\ell = 0.601$ Using $C_{N_\alpha} = 3.44$/radian

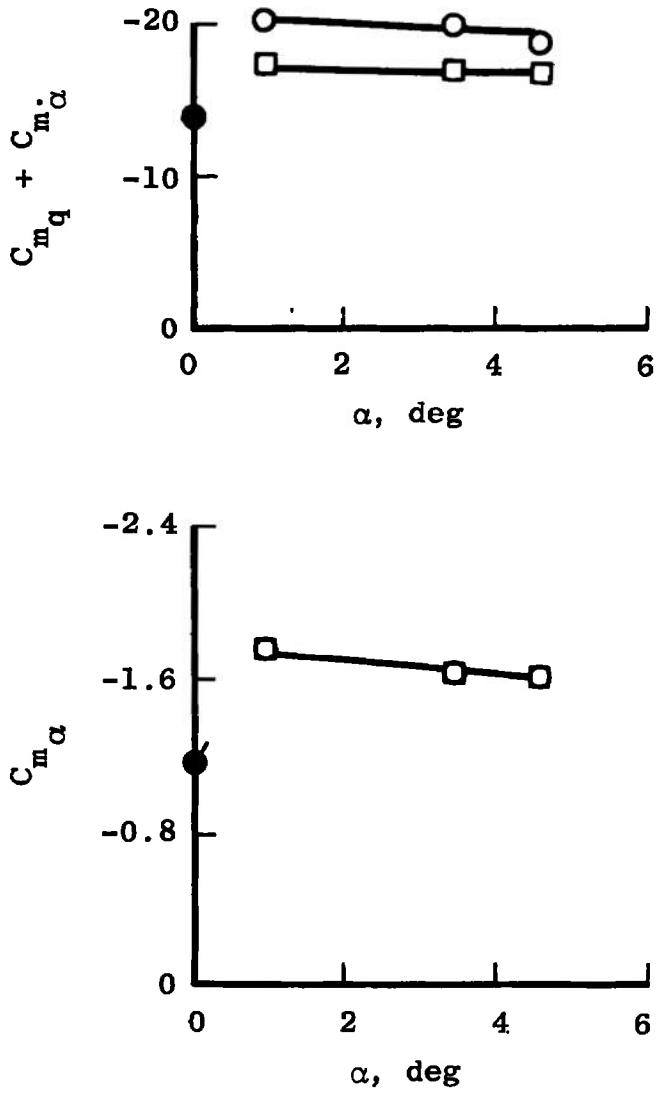

Fig. 12 Effect of Amplitude of Oscillation on the Dynamic- and Static-Stability Derivatives, Straight Wing Orbiter, Interference-Free Data

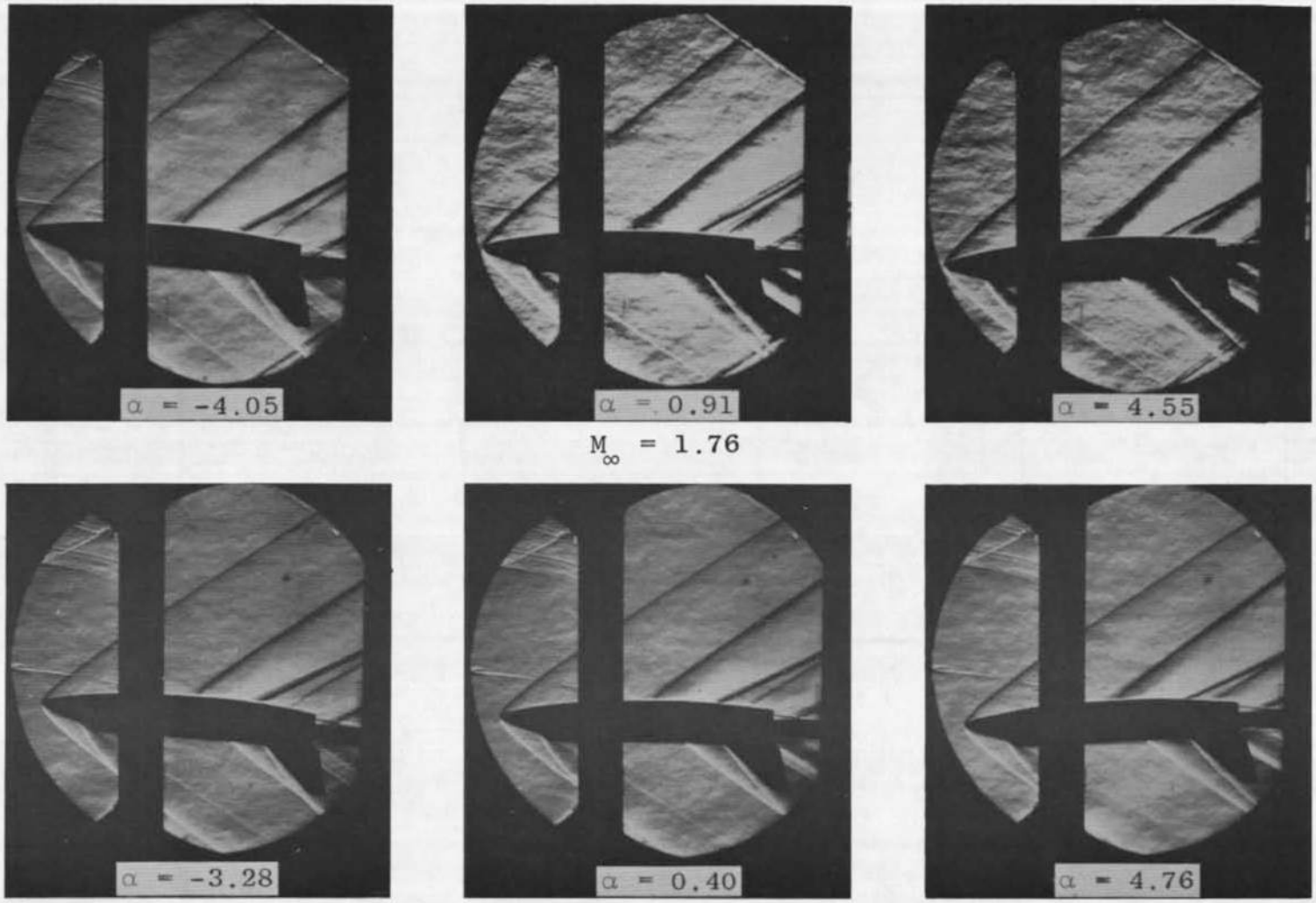

a. Interference Free

Fig. 13 Straight Wing Orbiter Schlieren Photographs

b. With Interference, M_∞ = 1.99
Fig. 13 Concluded

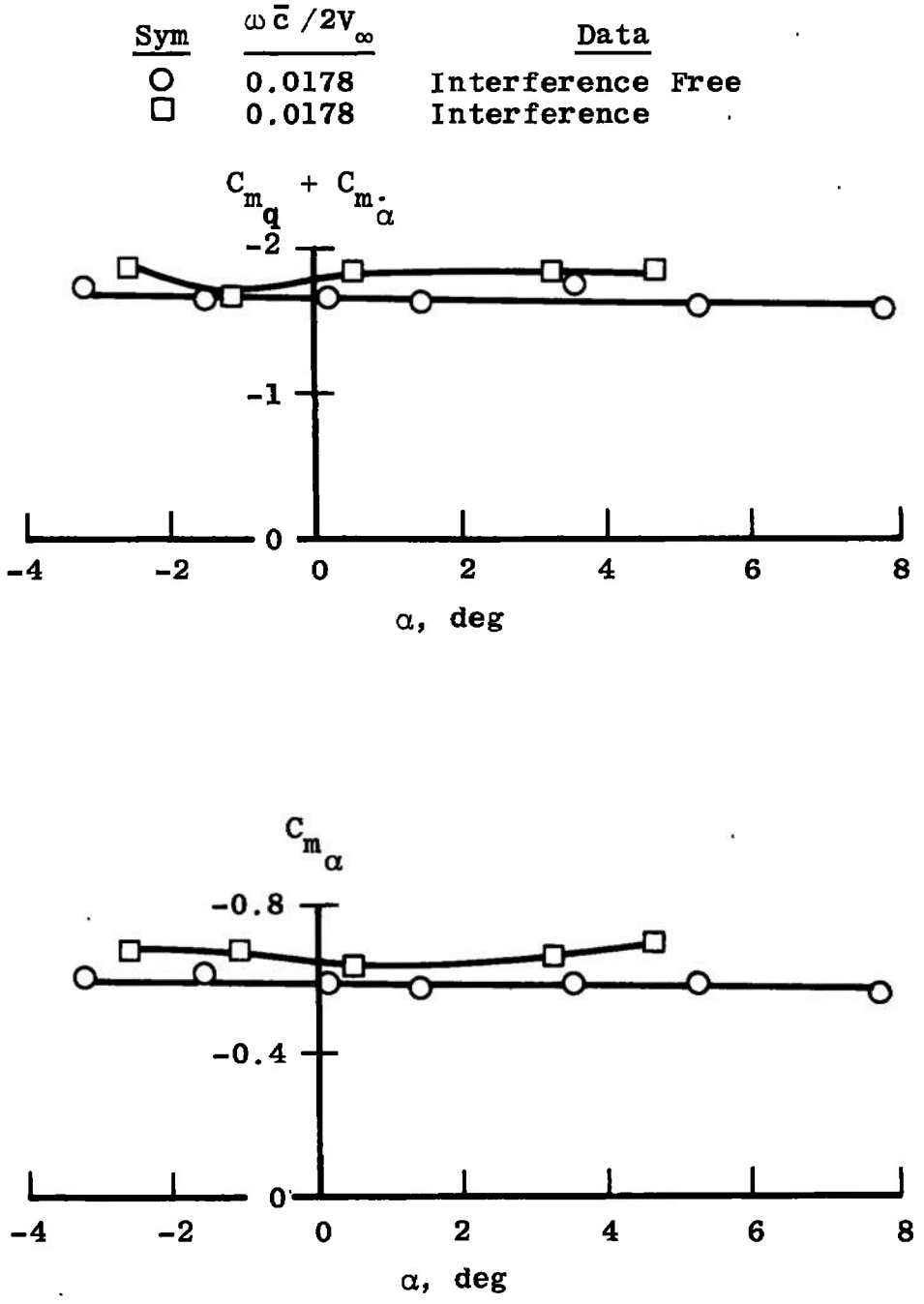

a. X/L ≈ 0.14, Z/L ≈ 0.15

Fig. 14 Dynamic- and Static-Stability Derivatives as a Function of Angle of Attack, Delta Wing Orbiter and Delta Wing Booster, $M_\infty = 2$, $Re_\ell \approx 2 \times 10^6$

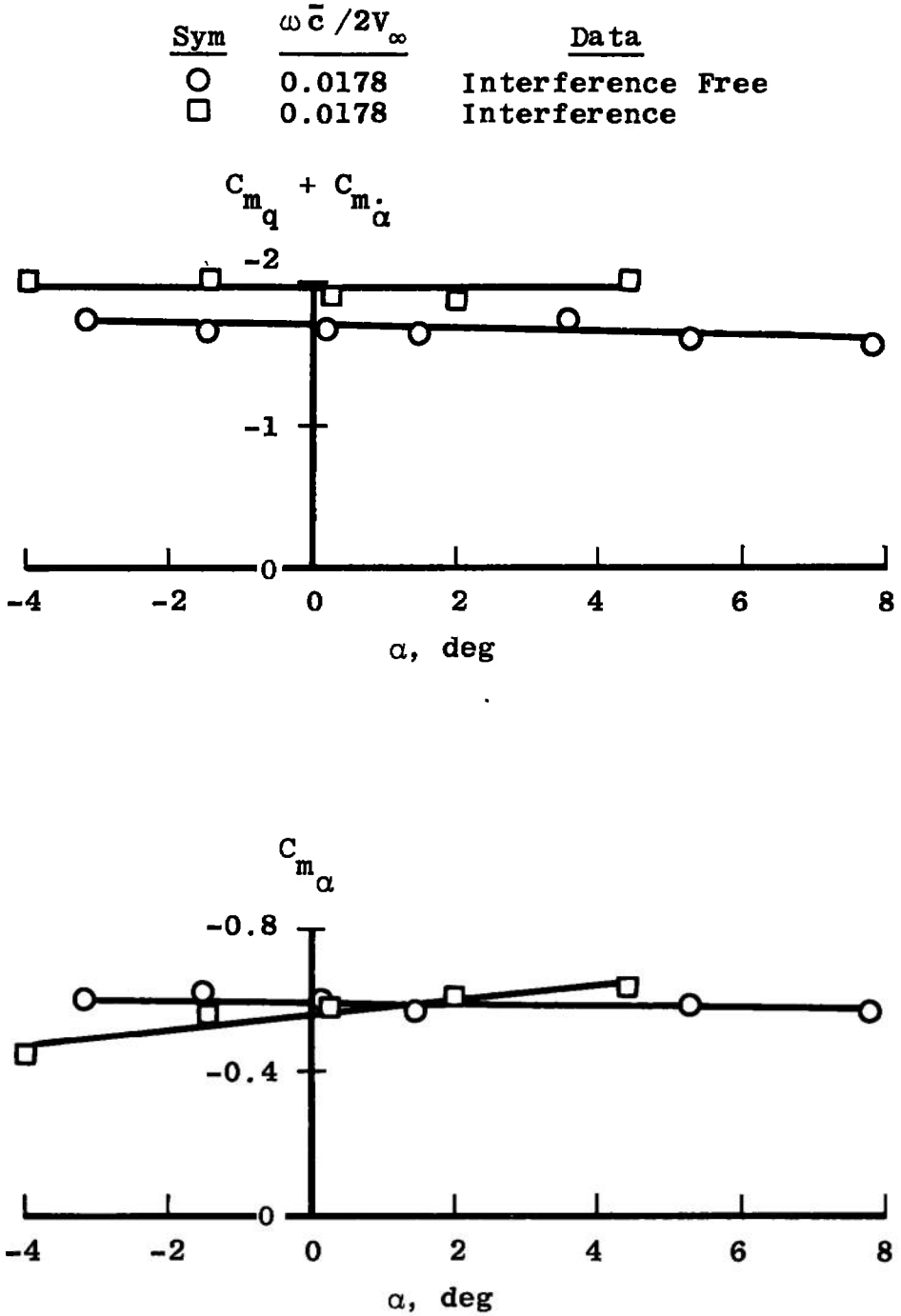

b. X/L ≈ 0.02, Z/L ≈ 0.15

Fig. 14 Continued

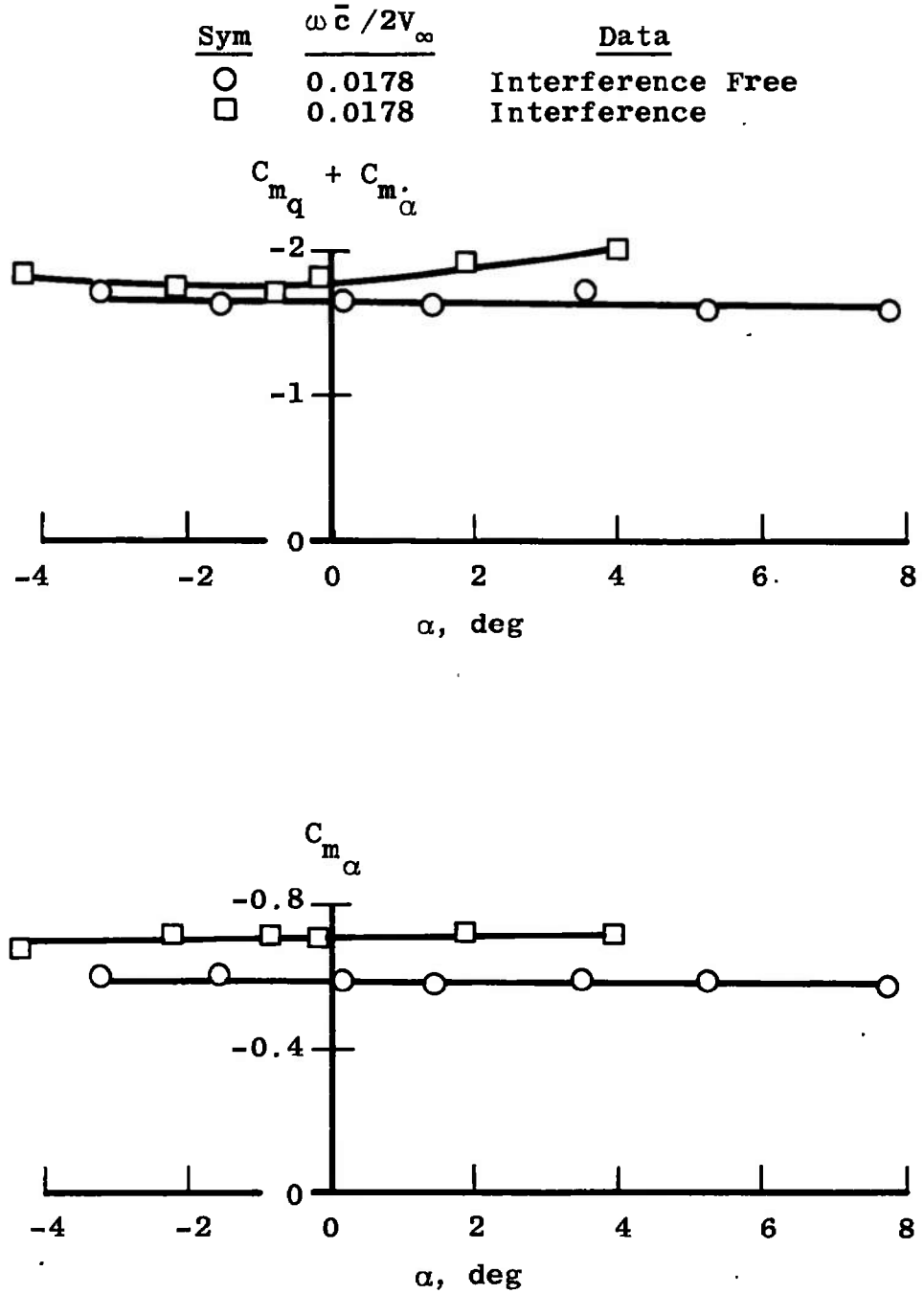

c. X/L ≈ -0.33, Z/L ≈ 0.15

Fig. 14 Continued

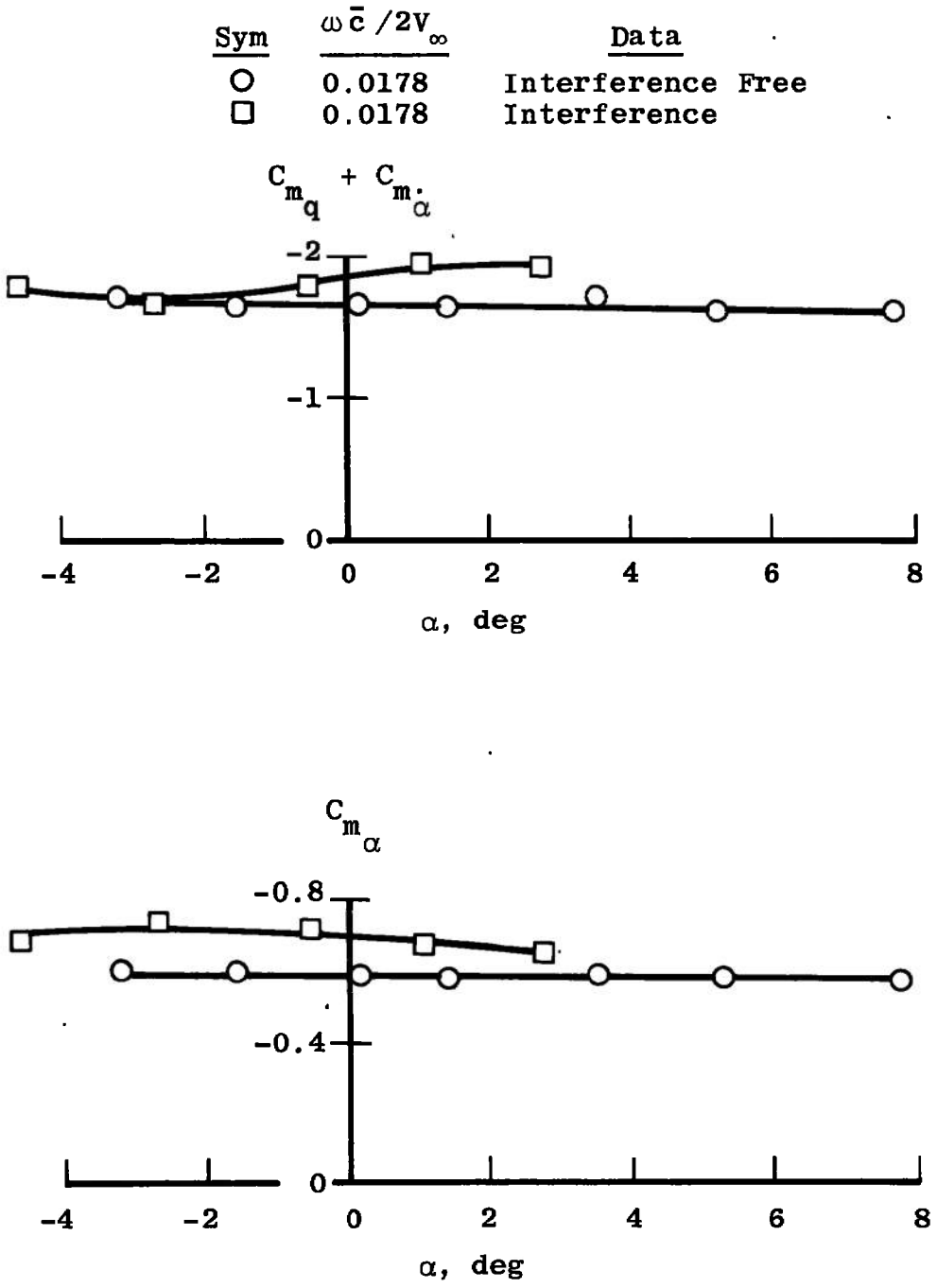

d. X/L ≈ 0.26, Z/L ≈ 0.35

Fig. 14 Continued

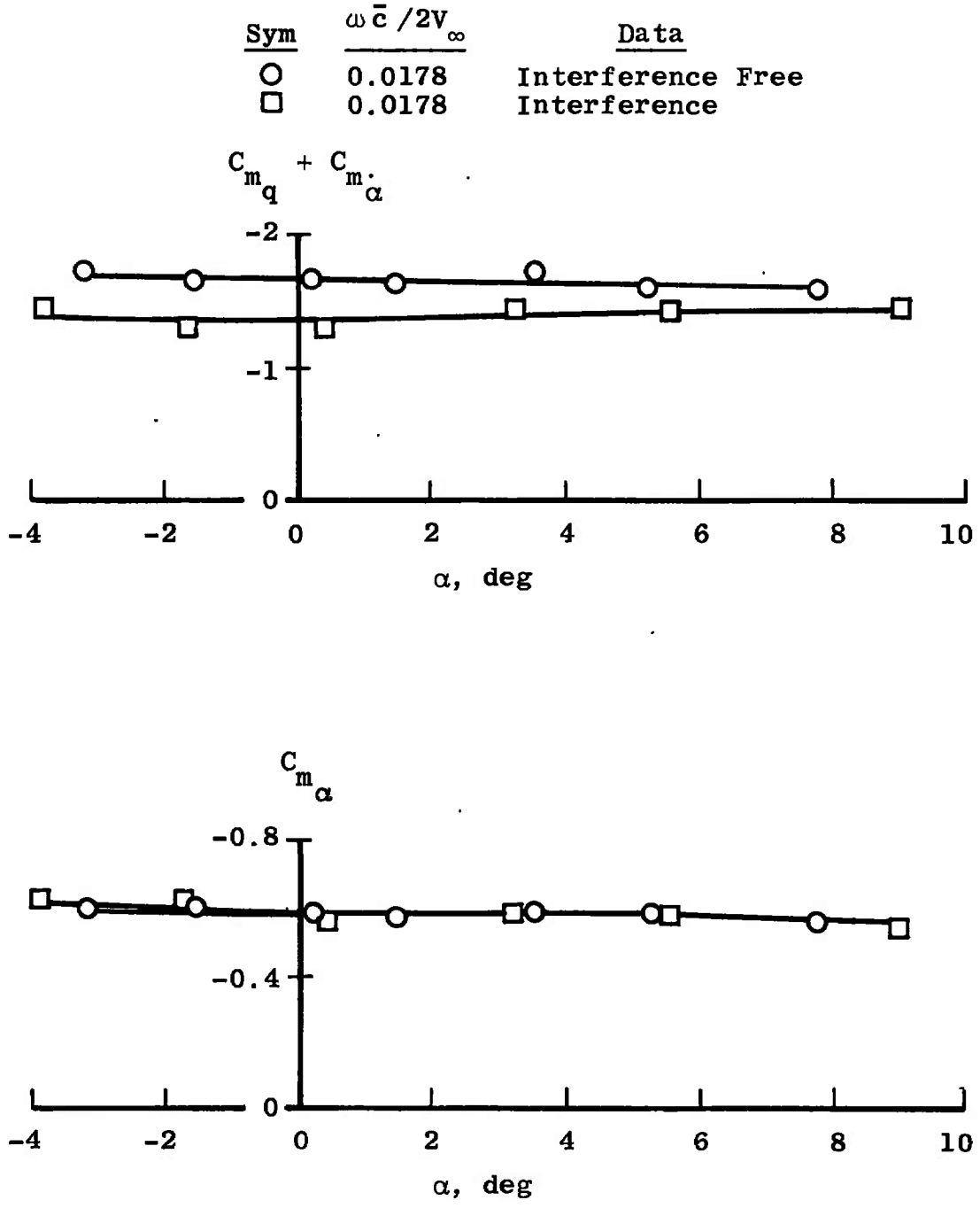

e. X/L ≈ 0, Z/L ≈ 0.35
Fig. 14 Continued

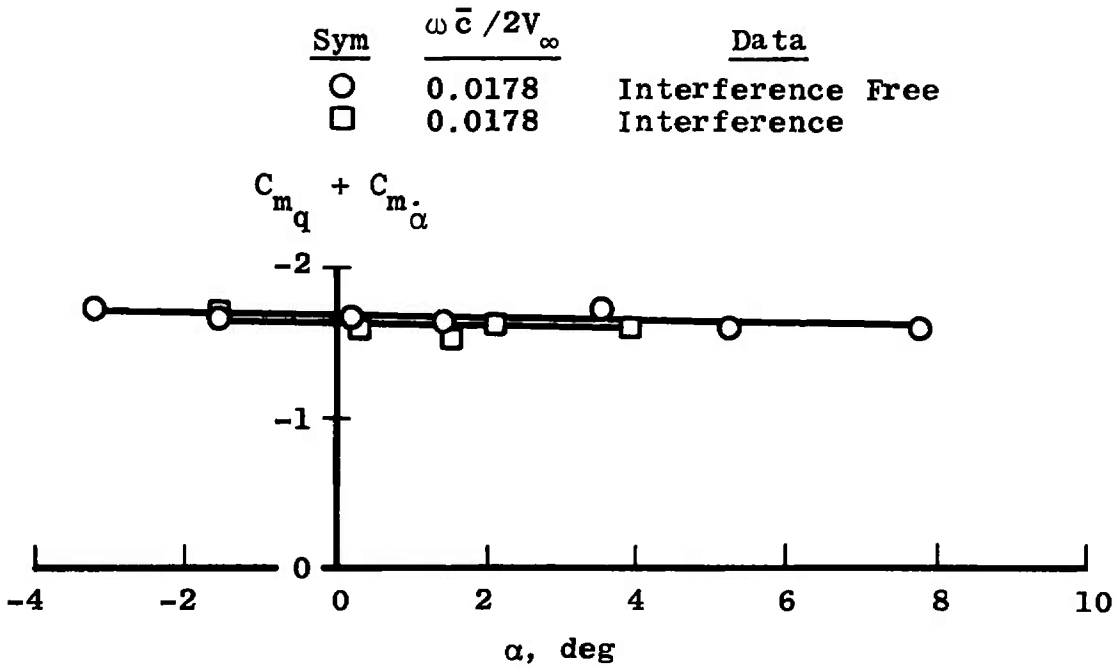

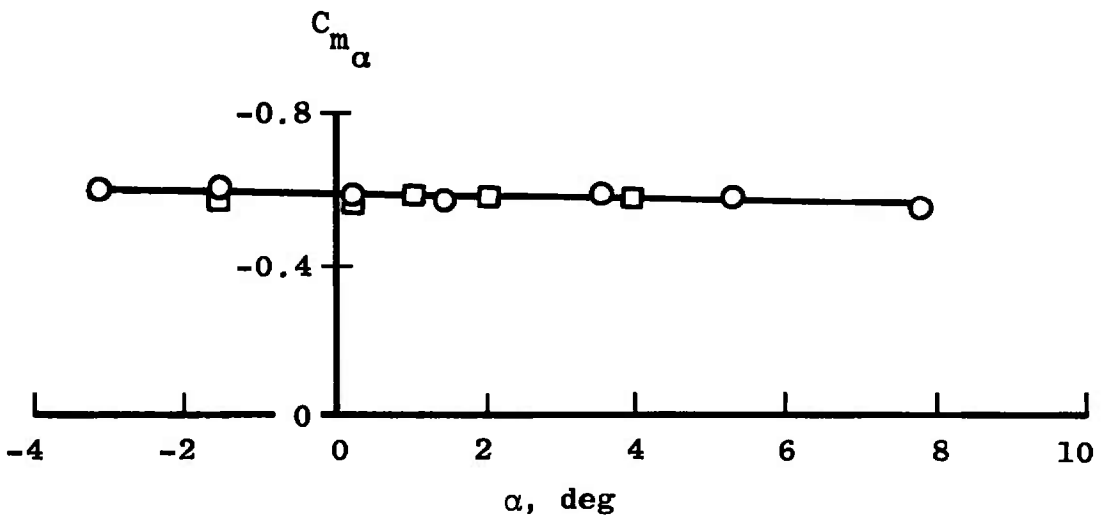

f. X/L ≈-0.29, Z/L ≈ 0.35

Fig. 14 Concluded

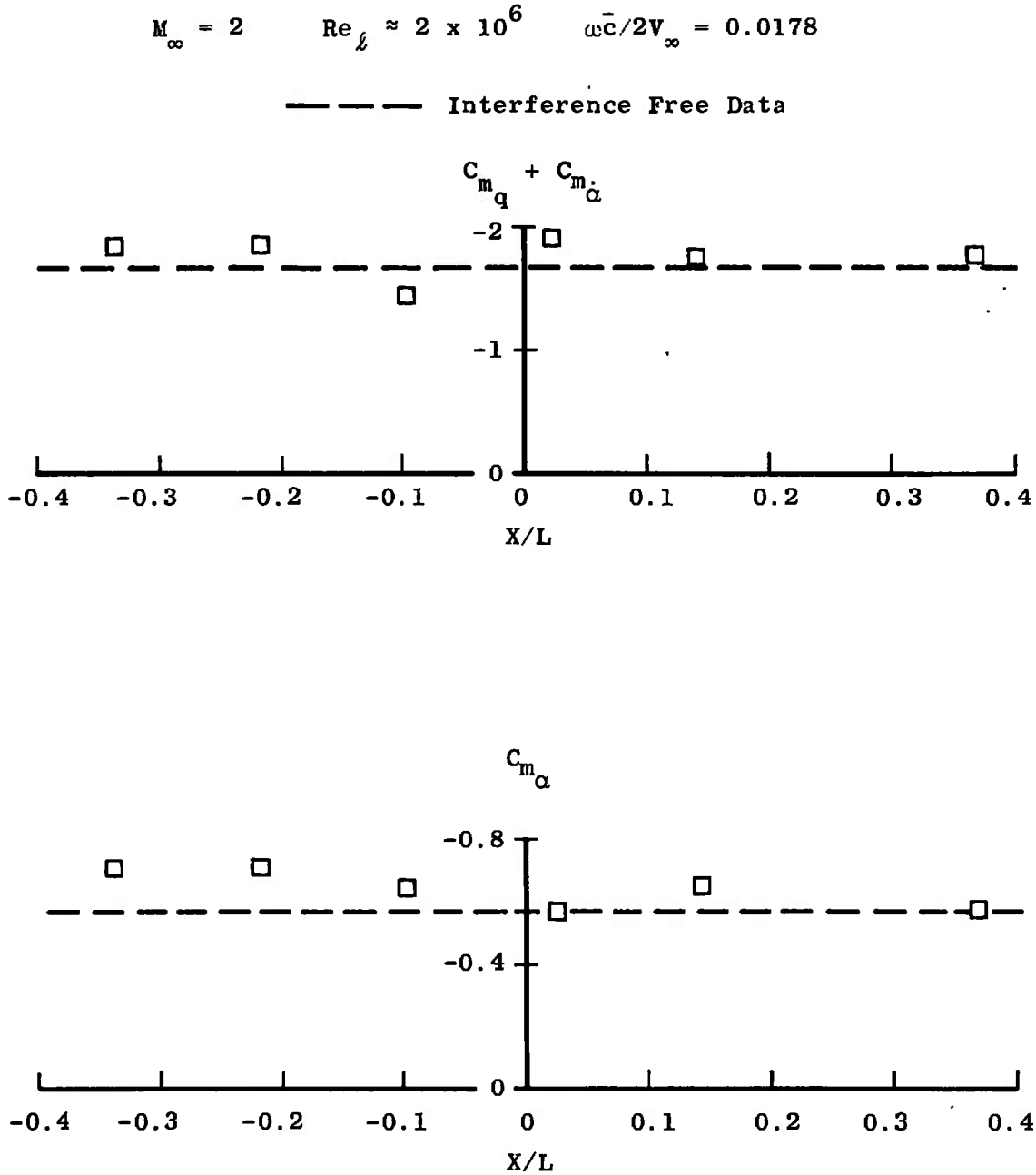

a. $\alpha = 0$

Fig. 15 Dynamic- and Static-Stability Derivatives as a Function of Relative Position of Orbiter and Booster, Delta Wing Orbiter and Delta Wing Booster, Z/L ≈ 0.15

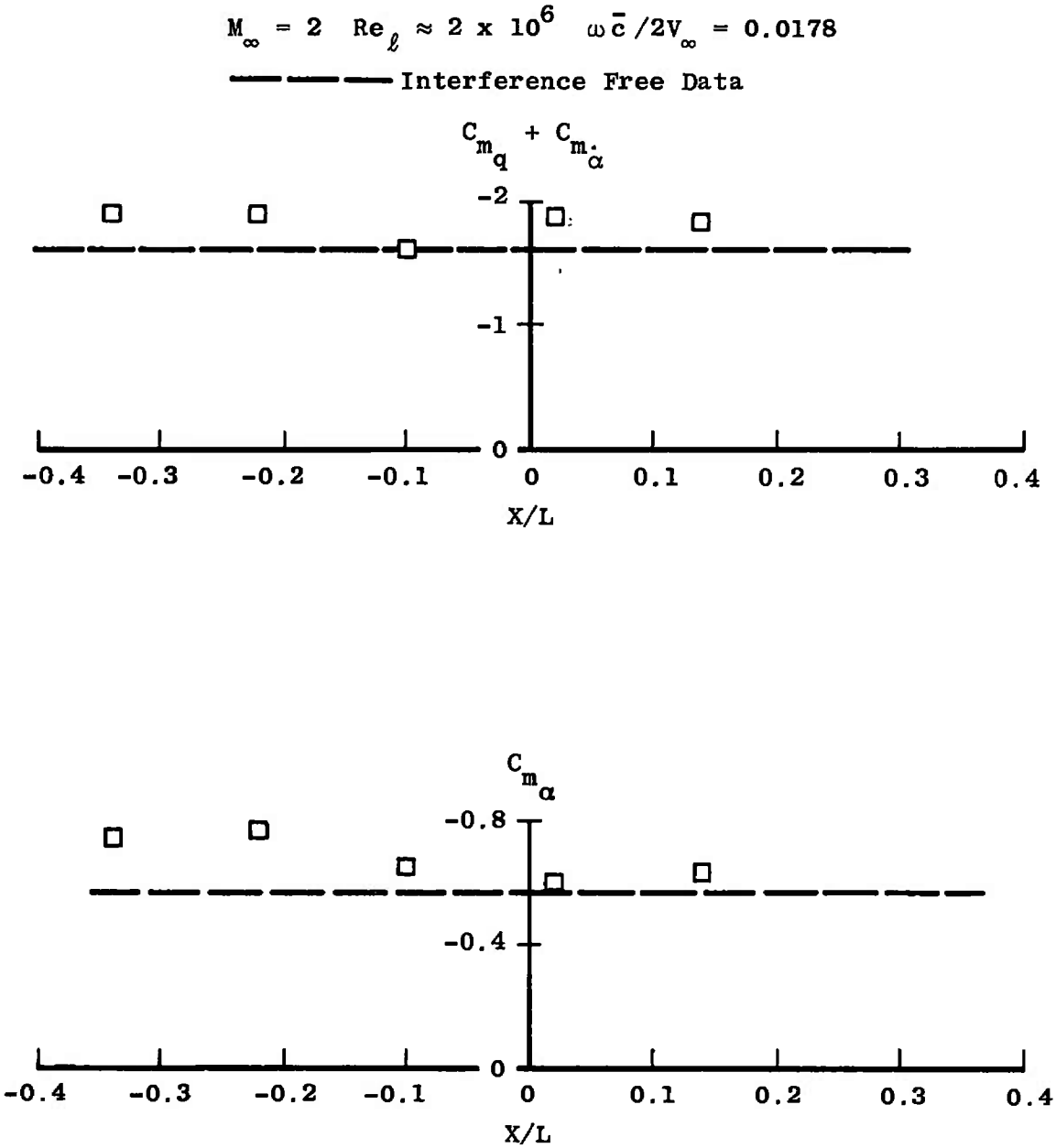

b. α = 2 deg

Fig. 15 Continued

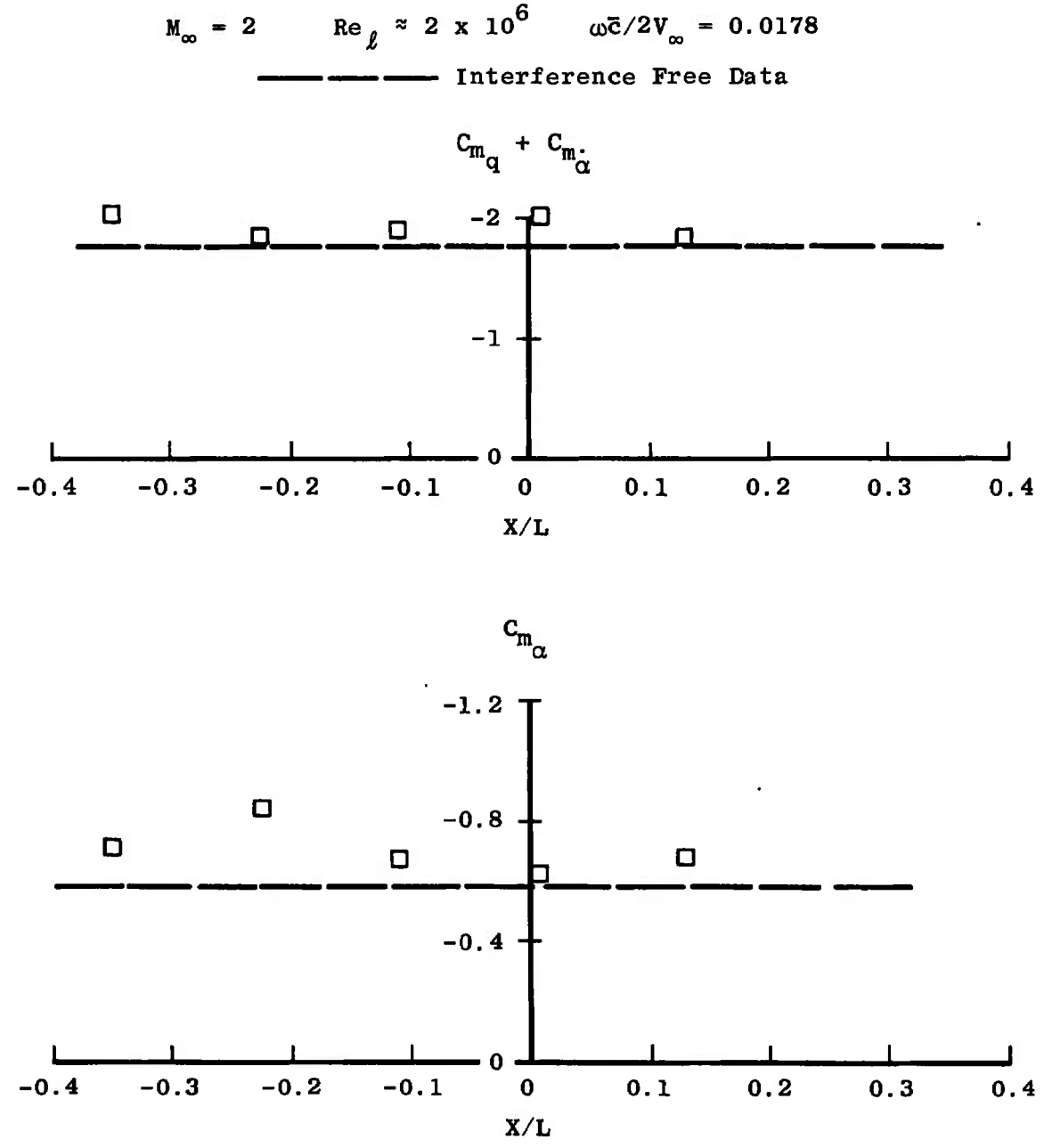

c. α = 4 deg
Fig. 15 Continued

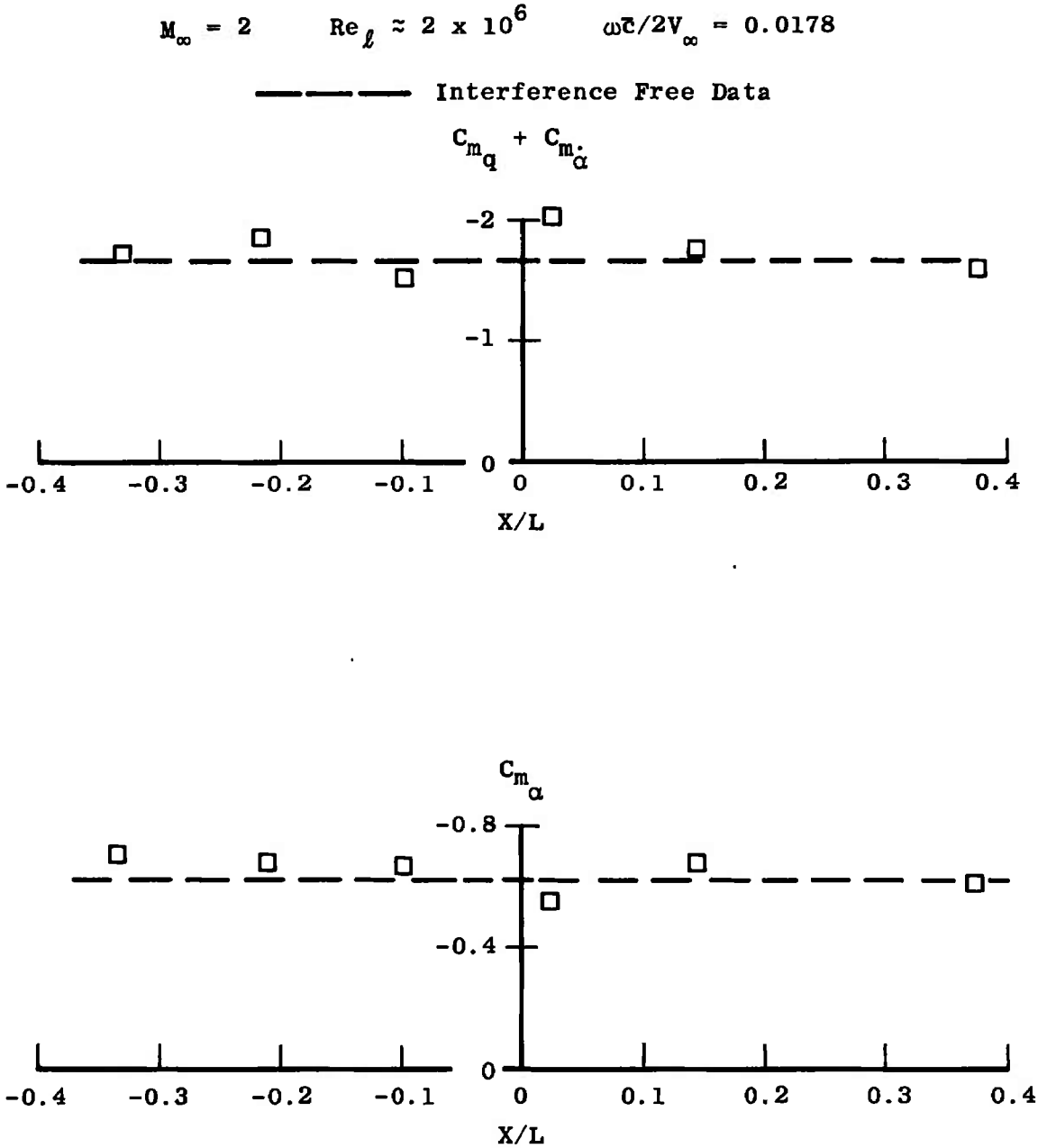

d. α =-2 deg

Fig. 15 Concluded

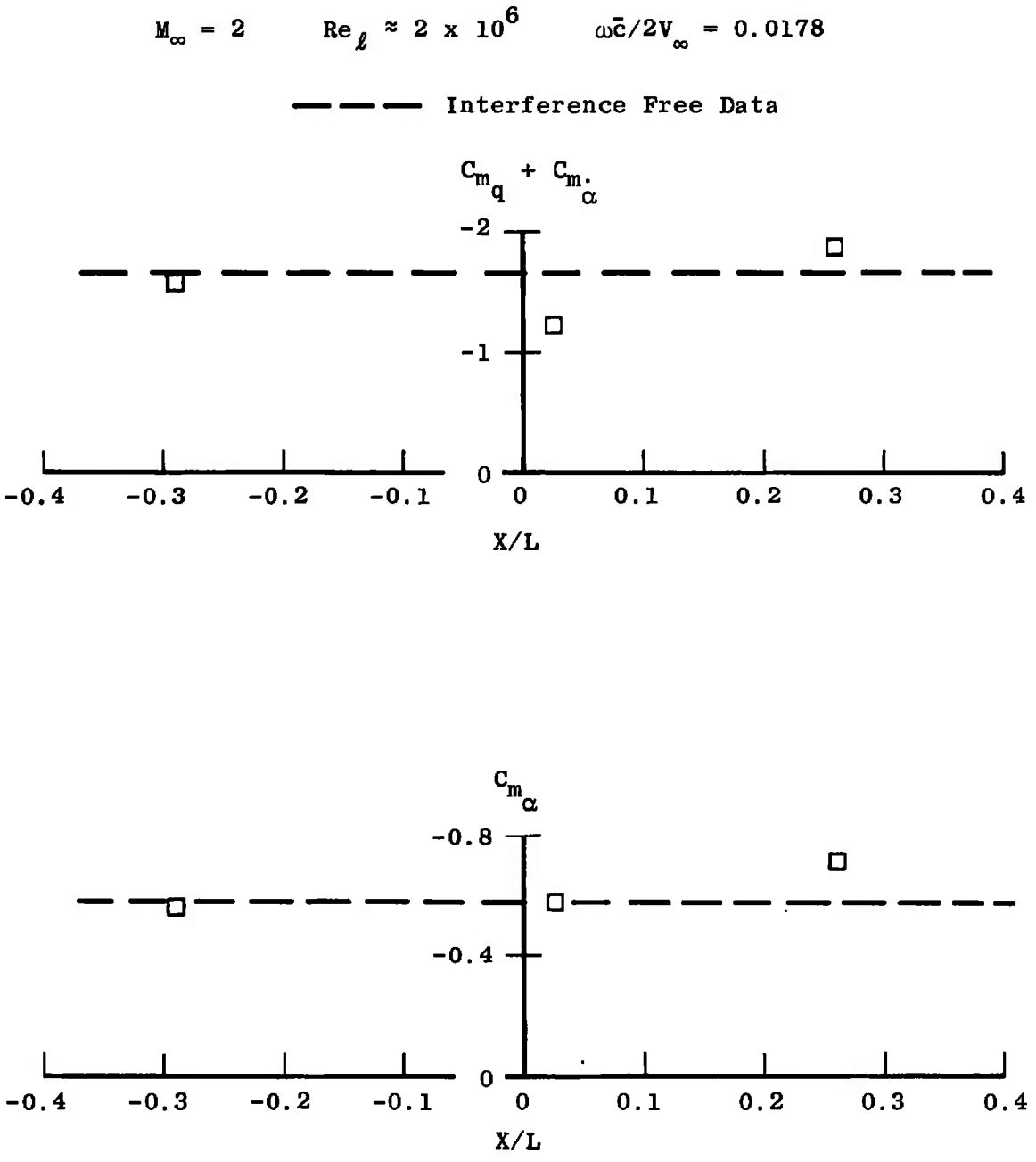

a. $\alpha = 0$

Fig. 16 Dynamic- and Static-Stability Derivatives as a Function of Relative Position of Orbiter and Booster, Delta Wing Orbiter and Delta Wing Booster, Z/L ≈ 0.35

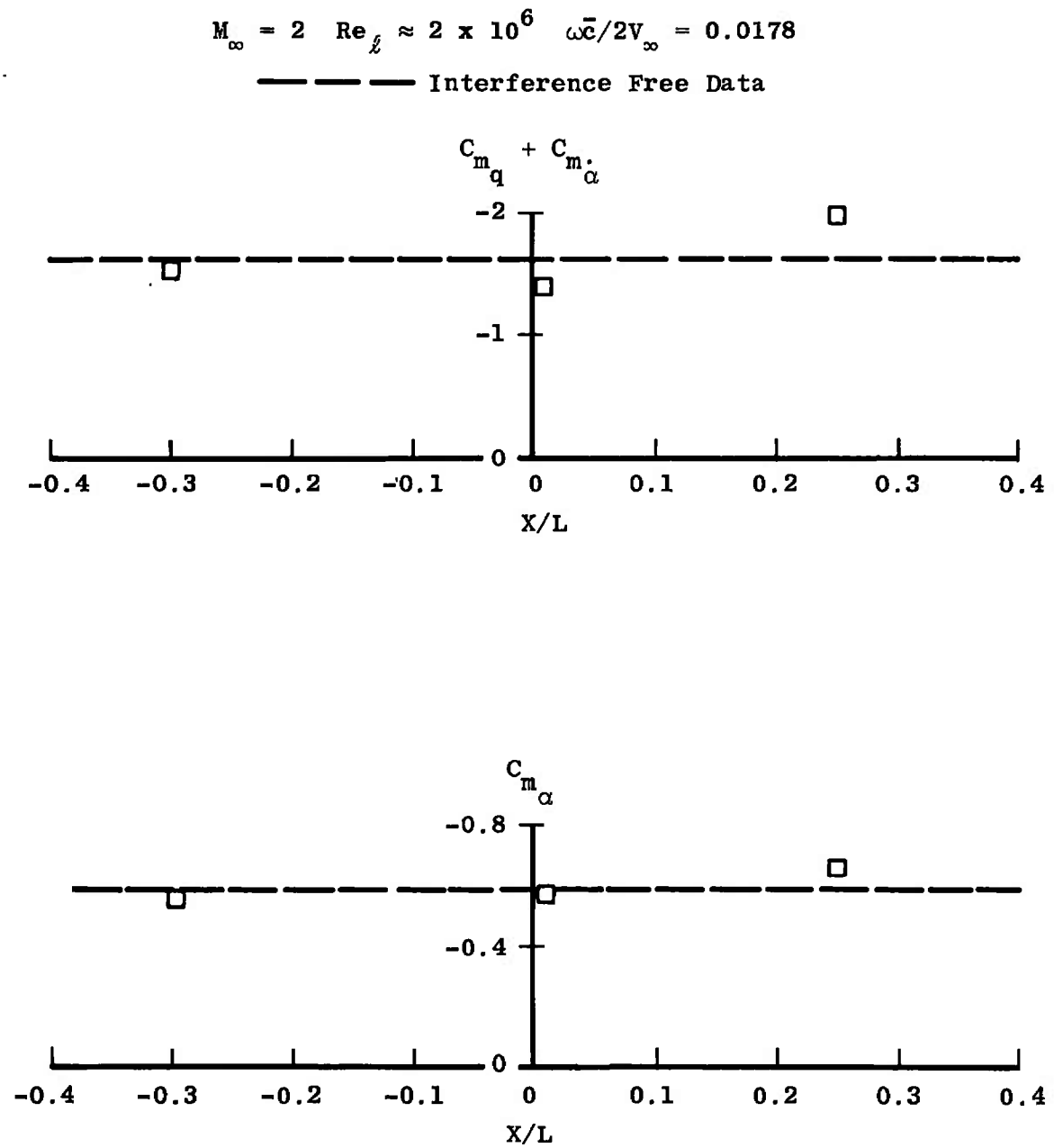

b. α = 2 deg

Fig. 16 Continued

$M_\infty = 2$ $\quad Re_\ell \approx 2 \times 10^6$ $\quad \omega\bar{c}/2V_\infty = 0.0178$

——— Interference Free Data

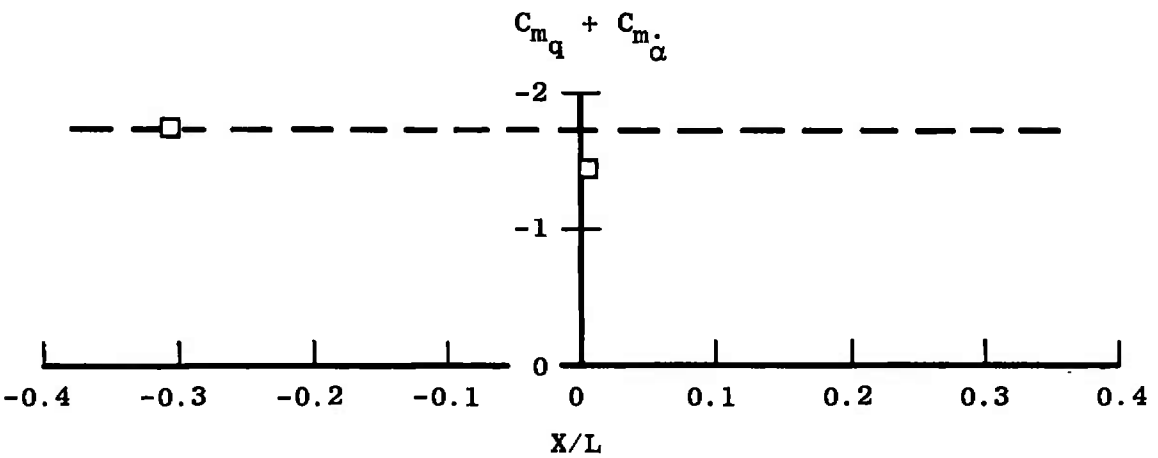

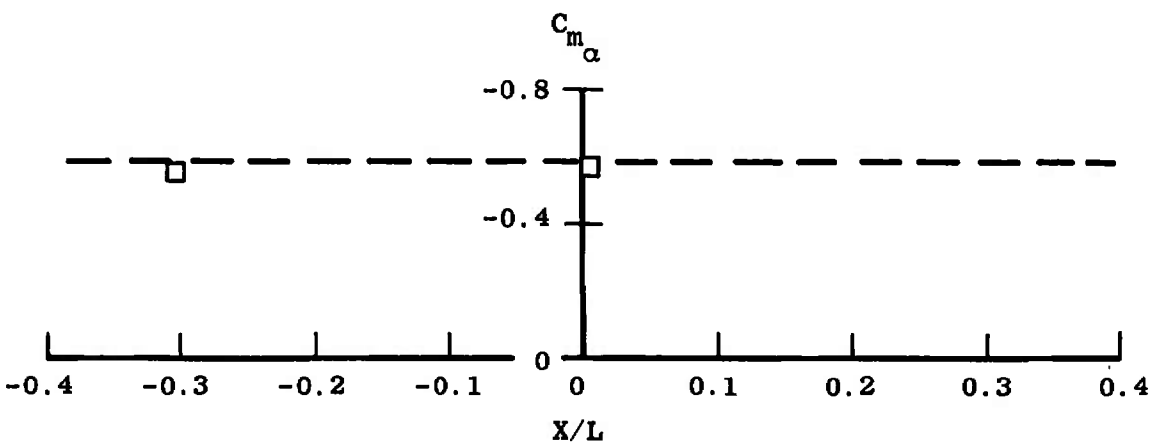

c. $\alpha = 4$ deg

Fig. 16 Continued

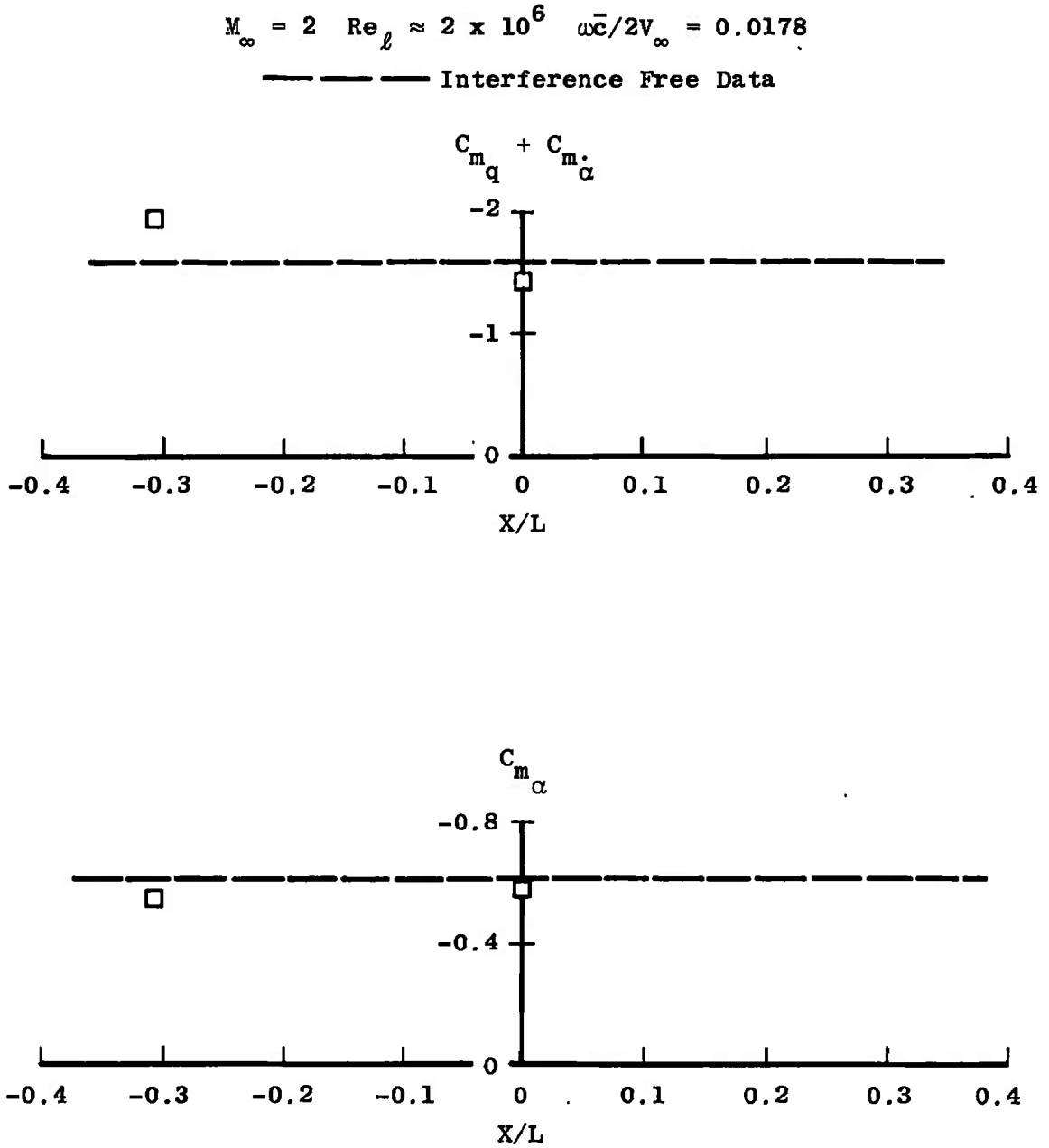

d. α = 6 deg

Fig. 16 Continued

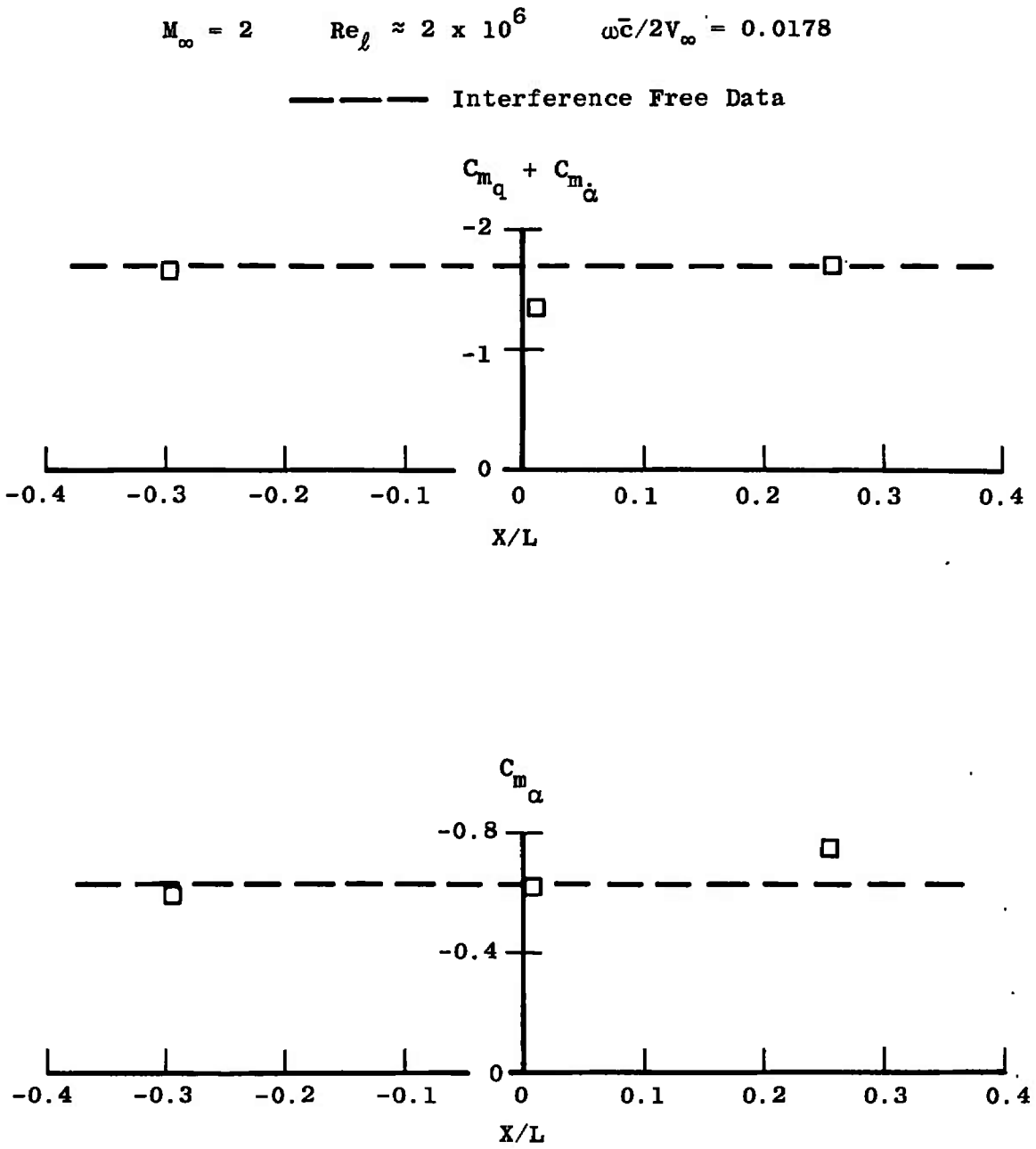

e. α = -2 deg

Fig. 16 Concluded

a. Interference Free

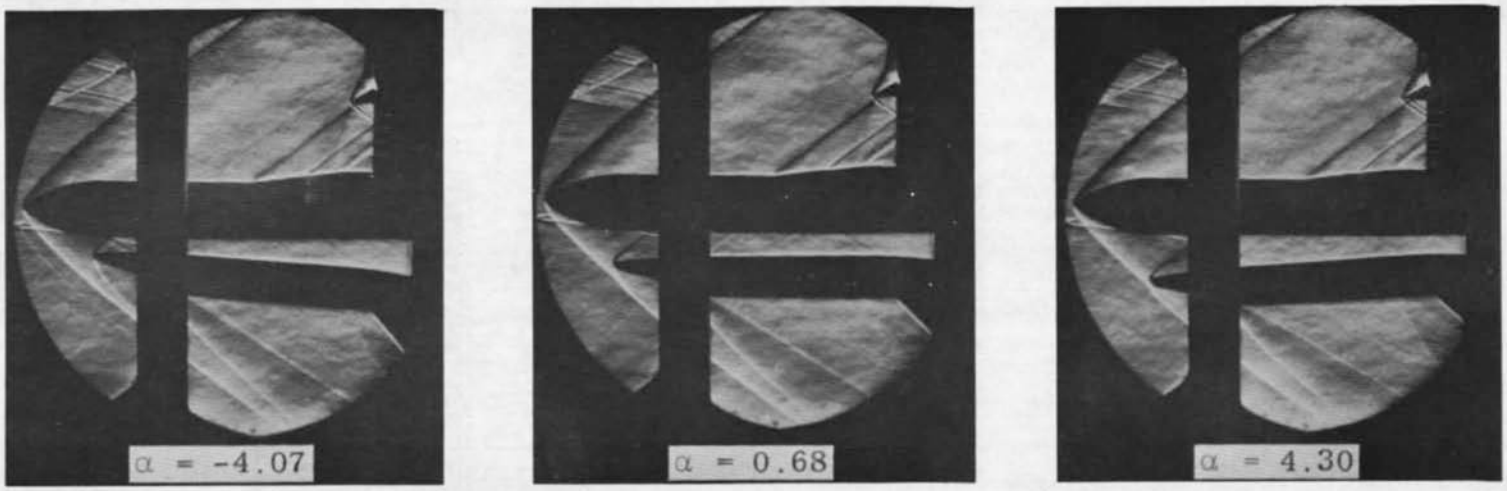

b. X/L ≈ -0.10, Z/L ≈ 0.152

Fig. 17 Delta Wing Orbiter Schlieren Photographs, M_∞ = 1.99

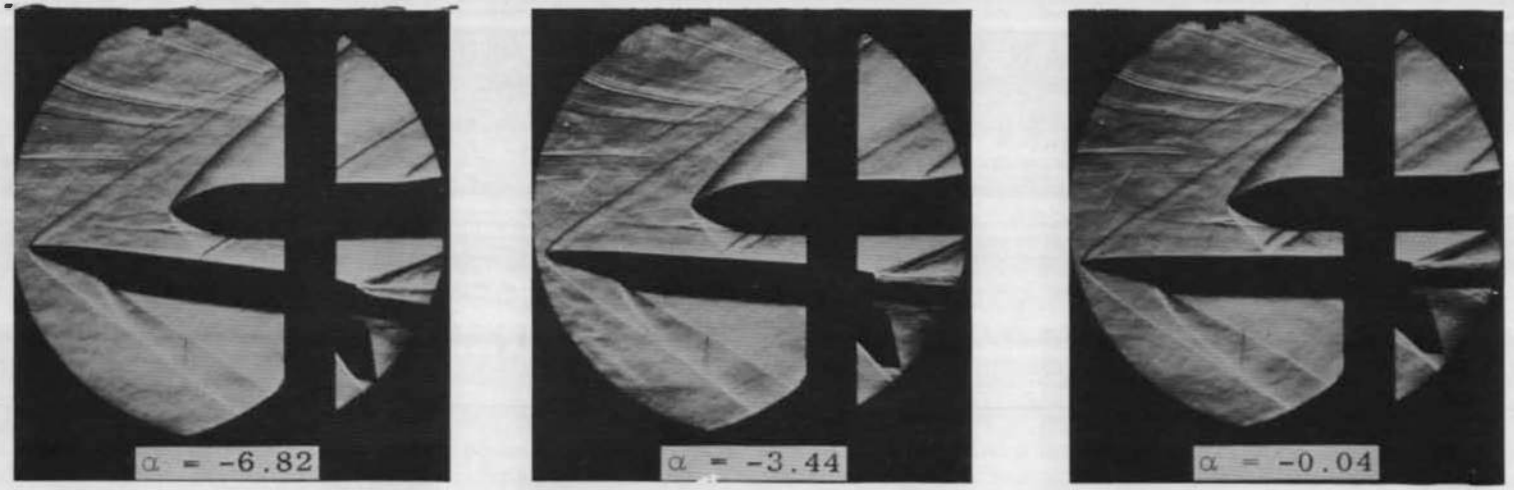

c. X/L ≈ 0.370, Z/L ≈ 0.152

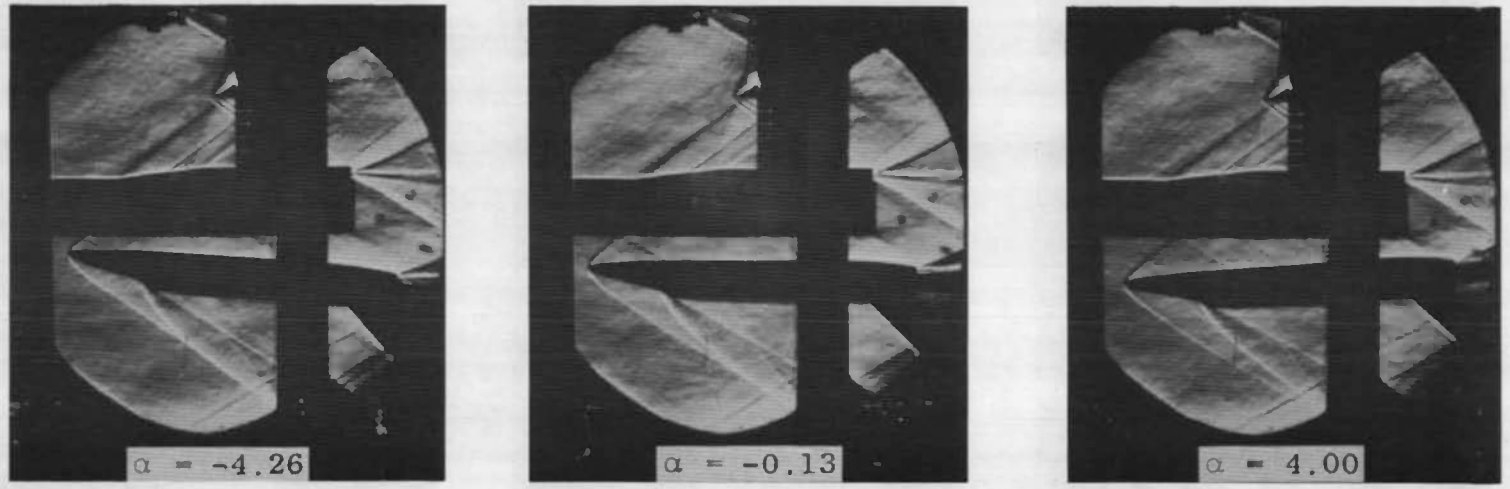

d. X/L ≈ -0.34, Z/L ≈ 0.152

Fig. 17 Continued

e. X/L ≈ 0.02, Z/L ≈ 0.150

f. X/L ≈ 0, Z/L ≈ 0.347

Fig. 17 Continued

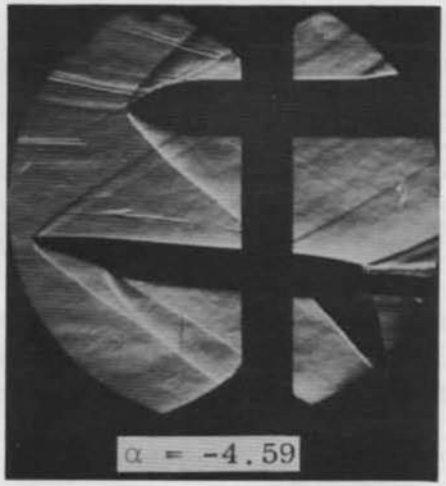

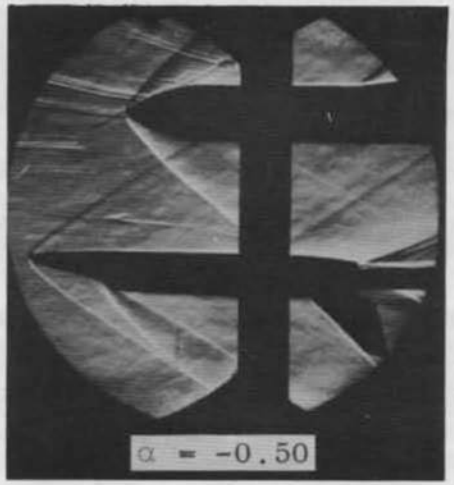

g. X/L ≈ 0.26, Z/L ≈ 0.347

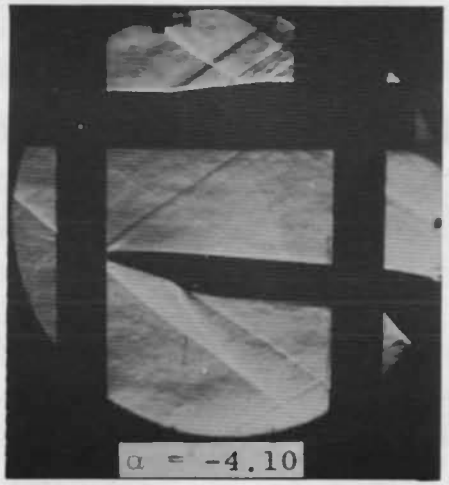

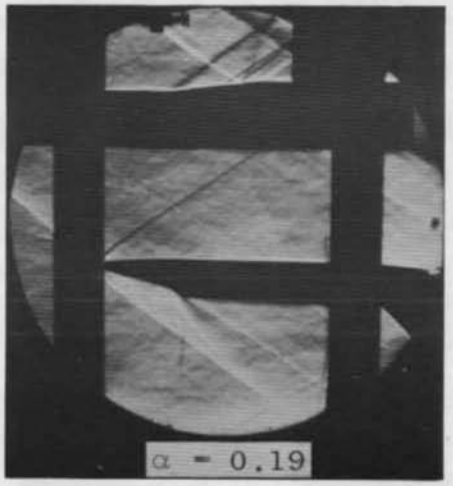

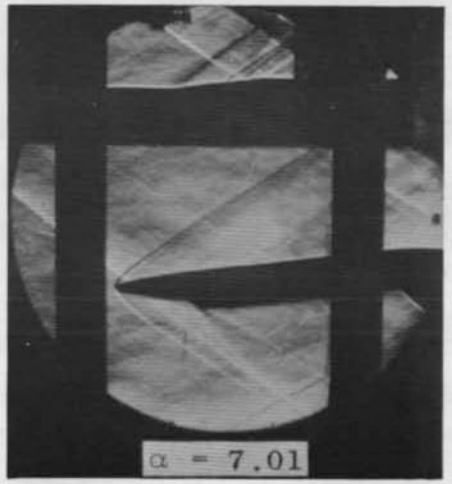

h. X/L ≈-0.30, Z/L ≈ 0.346

Fig. 17 Concluded

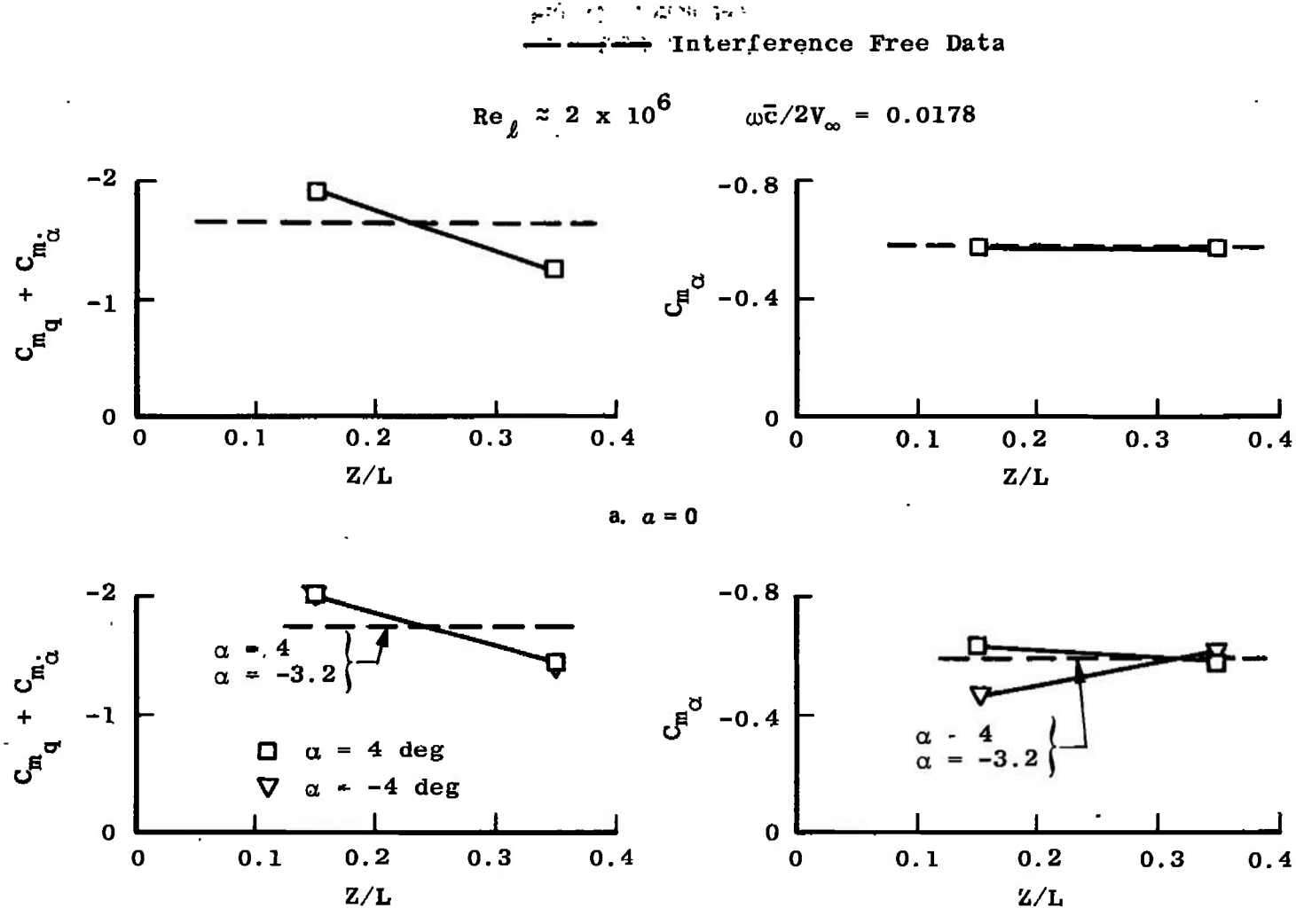

Fig. 18 Dynamic- and Static-Stability Derivatives as a Function of Relative Position of Orbiter and Booster, Delta Wing Orbiter and Delta Wing Booster, $M_\infty = 2$, $X/L \approx 0.02$

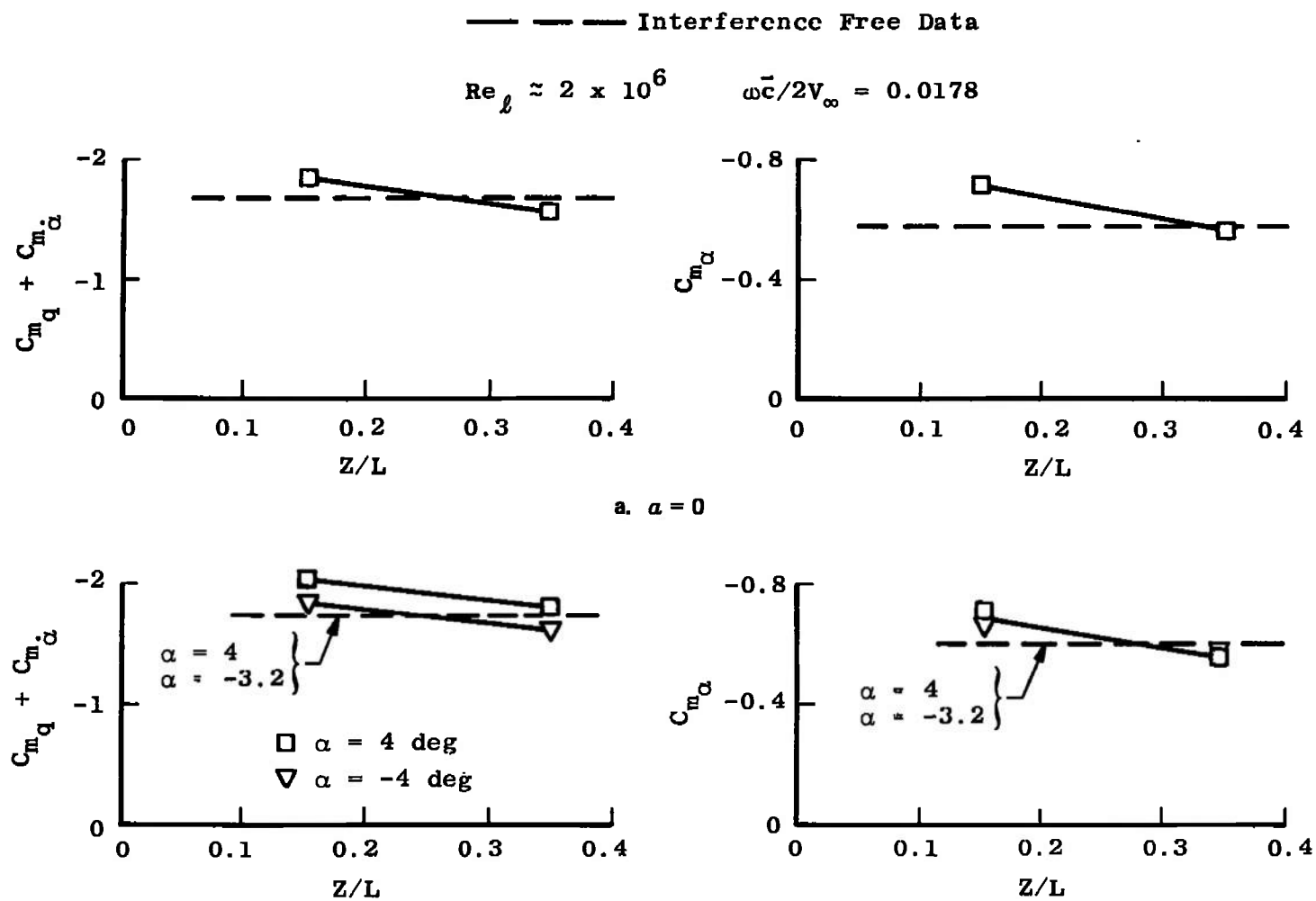

Fig. 19 Dynamic- and Static-Stability Derivatives as a Function of Relative Position of Orbiter and Booster, Delta Wing Orbiter and Delta Wing Booster, $M_\infty = 2$, X/L ≈-0.31

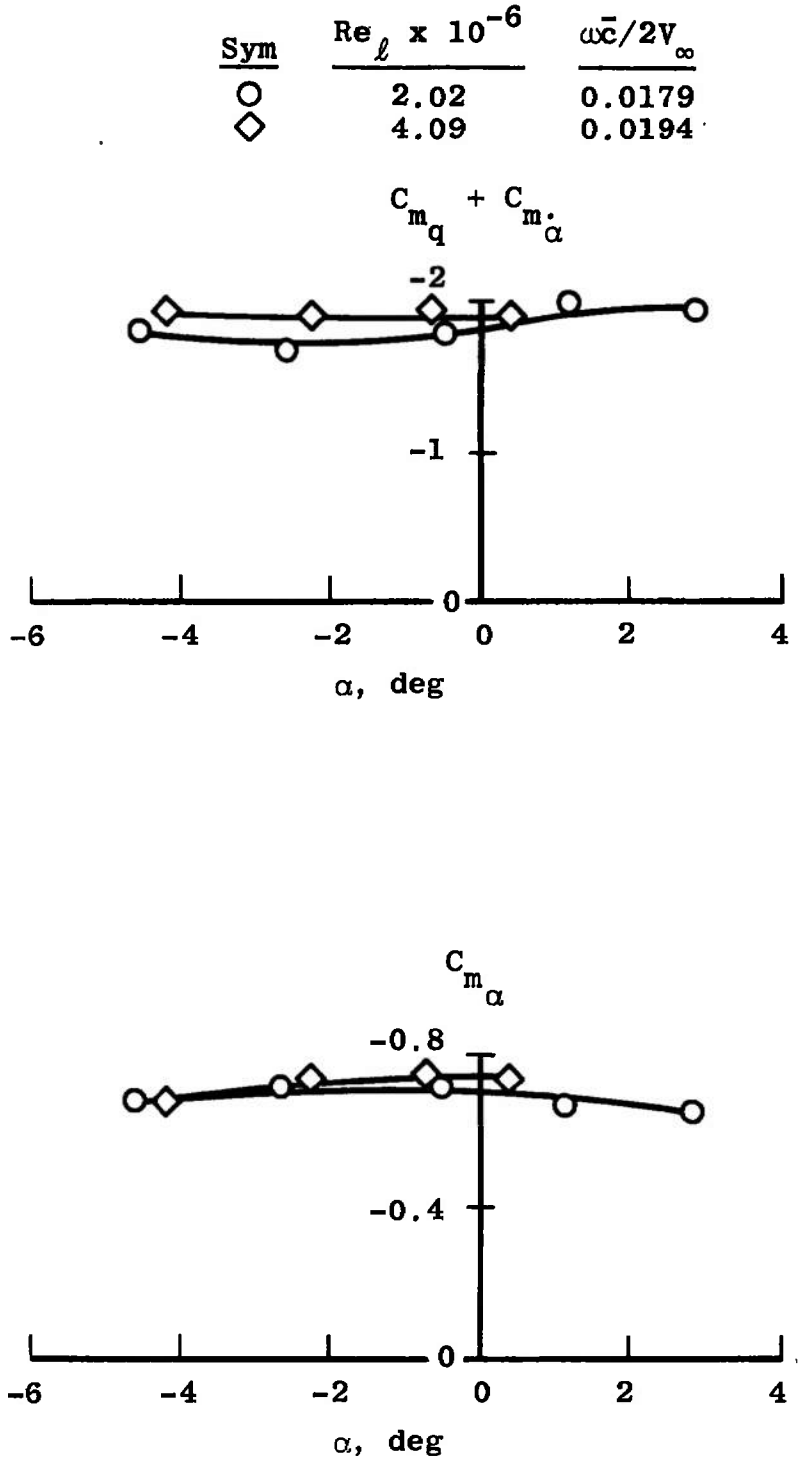

Fig. 20 Effect of Reynolds Number on Interference Data, Delta Wing Orbiter and Delta Wing Booster, X/L ≈ 0.26, Z/L ≈ 0.35, M_∞ = 2

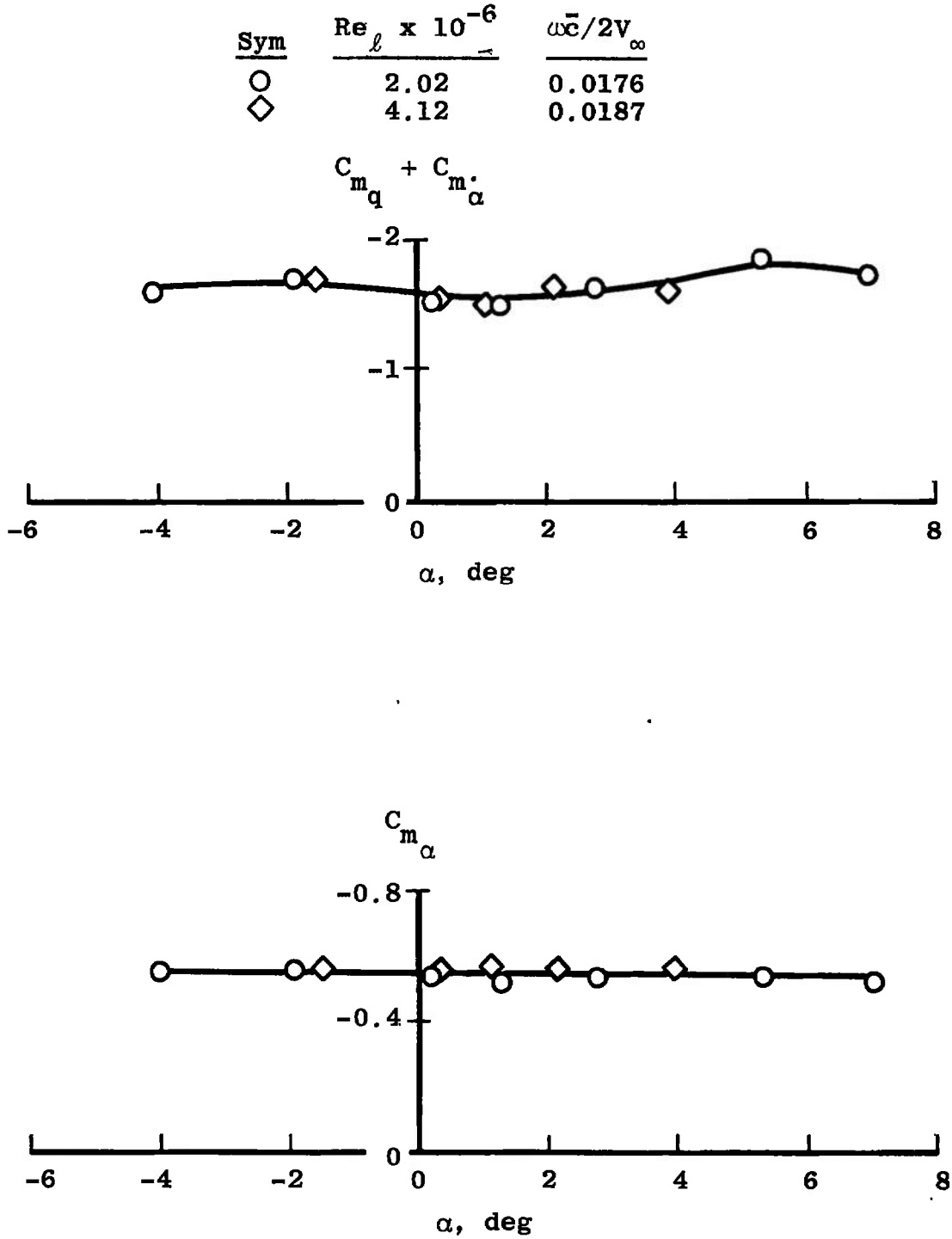

Fig. 21 Effect of Reynolds Number on Interference Data, Delta Wing Orbiter and Delta Wing Booster, X/L ≈ -0.3, Z/L ≈ 0.35, M_∞ = 2

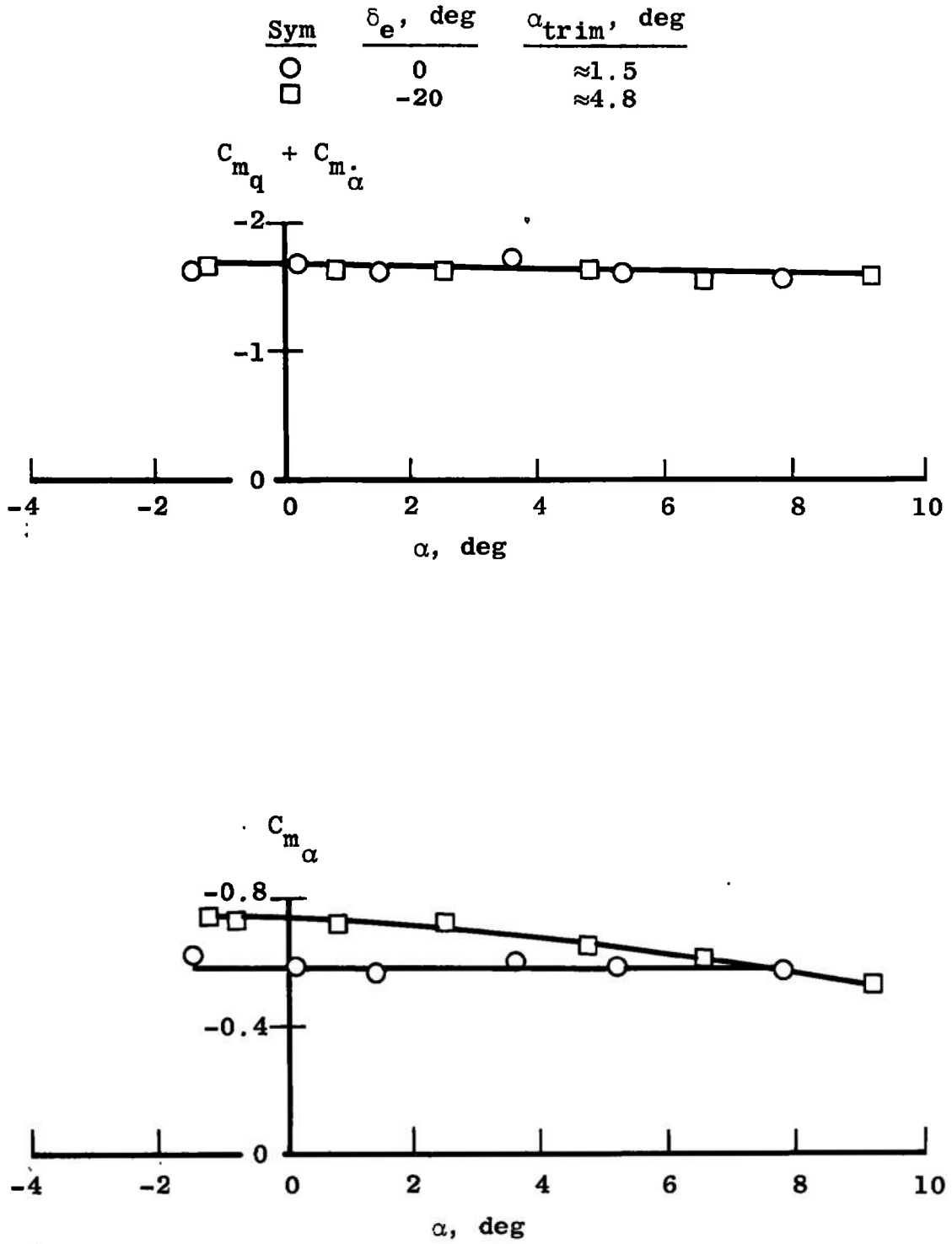

Fig. 22 Effect of Elevator Angle, Delta Wing Orbiter, Interference-Free Data, M_∞ = 2, Re_ℓ = 2.03 x 10^6

TABLE I
TEST SUMMARY

Configuration	Schedule	X/L	Z/L	δ_e deg	$\omega\bar{c}/2V_\infty$	α deg	α_{trim} deg
SWO	A	-	-	0	0.0071	-3.3 → 9.7	4.7
↓	C	-	-	0	0.0077	-4.0 → 9.5	3.8
↓	D	-	-	0	0.0080	-1.3 → 4.8	3.5
↓	E	-	-	0	0.0083	0.9 → 4.6	3.4
↓	E*	-	-	0	0.0083	0.9 → 4.6	3.4
DWO	A	-	-	0	0.0176	-3.2 → 7.8	1.5
↓	A	-	-	-20	0.0178	-1.2 → 9.2	4.8
DWO+DWB	A	-0.34	0.15	0	0.0179	-4.3 → 4.0	-0.8
↓	A	-0.22	0.15	0	0.0180	-4.1 → 4.0	0.4
↓	A	-0.10	0.15	0	0.0178	-4.1 → 4.3	0.7
↓	A	0.02	0.15	0	0.0177	-4.0 → 4.4	2.0
↓	A	0.14	0.15	0	0.0178	-2.6 → 4.7	3.2
↓	A	0.37	0.15	0	0.0177	-6.8 → 0	-0.4
↓	A	-0.29	0.35	0	0.0176	-4.1 → 7.0	1.3
↓	A	0.01	0.35	0	0.0177	-3.8 → 9.1	3.3
↓	A	0.26	0.35	0	0.0178	-4.6 → 2.8	-2.7
↓	B	-0.29	0.15	0	0.0194	-3.3 → 1.8	-0.6
↓	B	0.26	0.15	0	0.0191	0 → 3.0	3.0
↓	B	-0.29	0.35	0	0.0187	-1.5 → 3.9	1.1
↓	B	0.26	0.35	0	0.0193	-4.2 → 0.4	-2.3
SWO+DWB	A	-0.11	0.17	0	0.0071	-4.3 → 5.8	3.2
↓	A	0.20	0.17	0	0.0072	-3.9 → 7.3	7.2

*$\theta \approx \pm 1$ deg $\theta \approx \pm 1.6$ deg

Configuration Nomenclature

SWO - Straight Wing Orbiter Alone
DWO - Delta Wing Orbiter Alone
SWO+DWB - Straight Wing Orbiter in Proximity with Delta Wing Booster
DWO+DWB - Delta Wing Orbiter in Proximity with Delta Wing Booster

TABLE II
WIND TUNNEL TEST CONDITIONS

Schedule	M_∞	p_0 psia	T_0 °R	V_∞ ft/sec	q_∞ psia	Re_ℓ x 10-6
A	1.99	4.00	561	1726	1.44	2.03
B	2.00	8.04	560	1729	2.88	4.07
C	1.76	3.98	561	1606	1.60	2.10
D	1.76	8.00	560	1604	3.21	4.23
E	1.76	12.01	561	1606	4.81	6.33

UNCLASSIFIED

Security Classification

DOCUMENT CONTROL DATA - R & D

(Security classification of title, body of abstract and indexing annotation must be entered when the overall report is classified)

1. ORIGINATING ACTIVITY *(Corporate author)*
Arnold Engineering Development Center, Arnold Air Force Station, Tennessee 37389

2a. REPORT SECURITY CLASSIFICATION
UNCLASSIFIED

2b. GROUP
N/A

3 REPORT TITLE
DYNAMIC STABILITY TESTING OF SPACE SHUTTLE CONFIGURATIONS DURING ABORT SEPARATION AT MACH NUMBERS 1.76 AND 2

4 DESCRIPTIVE NOTES *(Type of report and inclusive dates)*
March 22 and 23, 1971--Final Report

5. AUTHOR(S) *(First name, middle initial, last name)*
Bob Uselton and Arthur R. Wallace, ARO, Inc.

6. REPORT DATE	7a. TOTAL NO. OF PAGES	7b. NO. OF REFS
October 1971	63	6

8a. CONTRACT OR GRANT NO.
Program Element 65802F

9a. ORIGINATOR'S REPORT NUMBER(S)
AEDC-TR-71-198

9b. OTHER REPORT NO(S) *(Any other numbers that may be assigned this report)*
ARO-VKF-TR-71-115

10. DISTRIBUTION STATEMENT
Approved for public release; distribution unlimited.

11. SUPPLEMENTARY NOTES
Available in DDC

12. SPONSORING MILITARY ACTIVITY
Arnold Engineering Development Center, Air Force Systems Command, Arnold Air Force Station, Tennessee

13. ABSTRACT Wind tunnel tests were conducted to determine the dynamic- and static-stability derivatives of an approximately 0.011-scale North American Rockwell straight wing and delta wing orbiters in proximity with an 0.011-scale General Dynamics/Convair delta wing booster. Interference-free data on the orbiter models were also obtained. Measurements were made with a forced-oscillation dynamic balance as the model oscillated ±1.6 deg at angles of attack ranging from -6.8 to 9.7 deg. Data were obtained at Mach numbers 1.76 and 2 and at free-stream Reynolds numbers, based on orbiter model length, ranging from 2.03×10^6 to 6.33×10^6. Both orbiter configurations were dynamically and statically stable, and in general, the level and trends of the orbiter derivatives were not greatly affected when in the proximity of the booster. The present damping data show fair agreement with damping data from the National Aeronautical Establishment (NAE), which are the only other known damping data of this type. However, the absolute level of the NAE C_{m_q} data, which were obtained using the half-model technique, was approximately 50 percent lower than that of the present data obtained on a three-dimensional model. Some disagreement was also found between the present static-stability data and data from the NASA-Ames and NASA-Langley test facilities.

DD FORM 1 NOV 65 1473

UNCLASSIFIED

Security Classification

14. KEY WORDS	LINK A		LINK B		LINK C	
	ROLE	WT	ROLE	WT	ROLE	WT
scale models						
spacecraft						
delta wings						
space flight						
Reynolds number						
supersonic flow						
abort separation						
dynamic stability						

AFSC
Arnold AFS Tenn